Forschungszentrum Karlsruhe
Technik und Umwelt

Wissenschaftliche Berichte
FZKA 5667

Overview Report of RAMONA-NEPTUN Program on Passive Decay Heat Removal

D. Weinberg, K. Rust, H. Hoffmann

Institut für Angewandte Thermo- und Fluiddynamik
Projekt Nukleare Sicherheitsforschung

März 1996

FORSCHUNGSZENTRUM KARLSRUHE
Technik und Umwelt

Wissenschaftliche Berichte
FZKA 5667

OVERVIEW REPORT OF RAMONA - NEPTUN PROGRAM ON PASSIVE DECAY HEAT REMOVAL

D. Weinberg, K. Rust, H. Hoffmann

Institut für Angewandte Thermo- und Fluiddynamik
Projekt Nukleare Sicherheitsforschung

Forschungszentrum Karlsruhe GmbH, Karlsruhe
1996

Forschungszentrum Karlsruhe GmbH
Postfach 3640, 76021 Karlsruhe

ISSN 0947-8620

OVERVIEW REPORT OF RAMONA - NEPTUN PROGRAM ON PASSIVE DECAY HEAT REMOVAL

ABSTRACT

The design of the advanced sodium-cooled European Fast Reactor provides a safety graded decay heat removal concept which ensures the coolability of the primary system by natural convection when forced cooling is lost. To assess the reliability of the passive safety system, many experiments were carried out in test facilities of different scale and detail using mainly water as the fluid simulant for convenience. An important requirement for the correct simulation of the natural convection and pool mixing process is to meet the similarity criteria of the thermodynamics. The group of water test facilities includes the setups RAMONA (360°, scale 1:20) and NEPTUN (360°, scale 1:5) of the Research Center Karlsruhe. Utilizing both setups, numerous experiments were performed under steady state conditions and in the transition range from forced to natural convection. All these investigations serve to prove the inherent safe removal of the decay heat, to study the physical processes taking place in the pool-type primary vessel and in the cooling circuits, and to provide data for the development, improvement, and assessment of computer programs such as the FLUTAN code. The FLUTAN code was used for the three-dimensional analysis of the combined fluid dynamics and heat transport and is provided to serve as tool to extrapolate from model investigations to prototype conditions.

During the course of the investigations, different design and operating parameters were studied; in particular: the design of the above core structure, the delayed startup time of the decay heat exchangers, the number of operating decay heat exchangers, the reduced fluid inventory of a three-loop model compared to a four-loop model, and the complete flow path blockage at the primary side of the intermediate heat exchangers.

The findings of the RAMONA and NEPTUN experiments indicate that the decay heat can be safely removed by natural convection. The operation of the decay heat exchangers being installed in the upper plenum causes the formation of a thermal stratification associated with a pronounced temperature gradient. The vertical extent of the stratification and the quantity of the gradient are depending on the fact whether a permeable or an impermeable shell covers the above core structure. A delayed startup time of the decay heat exchangers leads only to a slight increase of the temperatures in the upper plenum. A complete failure of half of the decay heat exchangers causes a higher temperature level in the primary system, but does not alter the global temperature distribution. The transient development of the temperatures is faster going on in a three-loop model than in a four-loop model

due to the lower amount of heat stored in the compacter primary vessel. If no coolant reaches the core inlet side via the intermediate heat exchangers, the core remains coolable. In this case, cold water of the upper plenum penetrates into the subassemblies (thermosyphon effects) and the interwrapper spaces existing in the NEPTUN core. The core coolability from above is feasible without any difficulty though the temperatures increase to a minor degree at the top end of the core. In this connection, the important role of the interstitial flow is demonstrated which contributes considerably to the heat removal from the core.

The thermal hydraulic computer code FLUTAN was applied for the 3D numerical simulation of the majority of the steady state RAMONA and NEPTUN tests as well as for selected transient RAMONA tests. The comparison of analytical against experimental data indicates a qualitatively and quantitatively satisfying agreement of the findings with respect to the field of isotherms as well as the temperature profiles in the upper plenum and within the region of the very complex NEPTUN core geometry.

ÜBERSICHTSBERICHT ZUM RAMONA - NEPTUN PROGRAMM ZUR PASSIVEN NACHWÄRMEABFUHR

KURZFASSUNG

Der Entwurf des fortgeschrittenen natriumgekühlten europäischen Schnellen Reaktors sieht ein sicherheitstechnisches System zur Nachwärmeabfuhr (NWA) vor, das die Kühlbarkeit des Primärsystems durch Naturkonvektion sicherstellt, wenn die Kühlung durch Zwangskonvektion nicht zur Verfügung steht. Zum Nachweis der Funktionstüchtigkeit dieses passiven NWA-Systems wurden umfangreiche Untersuchungen durchgeführt. Aus praktischen Gründen wurde häufig Wasser anstelle von Natrium als Kühlmittel verwendet. Die verwendeten Versuchseinrichtungen unterschieden sich sowohl im Maßstab als auch im Detaillierungsgrad. Um eine möglichst korrekte Simulation der Naturkonvektion und der Mischprozesse bei den Versuchen zu erzielen, müssen die Ähnlichkeitsgesetze der Thermodynamik weitgehend erfüllt werden. Zu den Prüfständen mit Wasserkühlung gehören die Versuchseinrichtungen RAMONA (360°, Maßstab 1:20) und NEPTUN (360°, Maßstab 1:5) des Forschungszentrums Karlsruhe. Beide Modelle wurden verwendet zur Durchführung von stationären Modell-Experimenten sowie von transienten Untersuchungen im Übergangsbereich von Zwangs- zu Naturkonvektion. Ziele dieser Versuche sind der Nachweis einer inhärent sicheren Abfuhr der Nachwärme, die Untersuchung der physikalischen Vorgänge im pool-förmigen Primärsystem und in den Kühlkreisläufen sowie die Erstellung von Daten zur Entwicklung, Verbesserung und Validierung von Rechenprogrammen, wie z.B. des FLUTAN Programms. Das FLUTAN Rechenprogramm wurde angewendet zur drei-dimensionalen Analyse der thermo- und fluiddynamischen Vorgänge und ist vorgesehen für die Extrapolation von Versuchsergebnissen auf prototypische Bedingungen.

Die Untersuchungen erstreckten sich im einzelnen auf folgende unterschiedliche Geometrie- und Betriebsparameter: Die Geometrie des Instrumentierungsstopfens, die verzögerte Inbetriebnahme der Tauchkühler und damit der Nachwärmeabfuhr, die Anzahl der betriebsfähigen Kühlkreisläufe zur Nachwärmeabfuhr, das reduzierte Kühlmittelvolumen einer Versuchsanlage mit drei Kühlkreisläufen im Vergleich zu einer solchen mit vier Kreisläufen sowie die vollständige Blockade der Strömungspfade auf der Primärseite der Zwischenwärmetauscher.

Die Ergebnisse der RAMONA und NEPTUN Experimente zeigen, daß die Nachwärme zuverlässig durch Naturumlauf abgeführt werden kann. Der Betrieb der Tauchkühler, die im Oberplenum angeordnet sind, bewirkt die Ausbildung einer horizontalen thermischen Stratifizierung mit einem ausgeprägten Temperaturgradienten. Die vertikale Ausbreitung der Schichtung sowie die Größe des Temperaturgradienten werden beeinflußt durch die Gestaltung des Instrumentie-

rungsstopfens mit durchströmbarer bzw. nicht durchströmbarer Ummantelung. Die verzögerte Inbetriebnahme der Tauchkühler verursacht geringfügig höhere Temperaturen im Oberplenum. Der Ausfall der Hälfte der installierten Tauchkühler führt zwar zu einem höheren Temperaturniveau im Oberplenum und damit im Primärsystem, verändert aber die allgemeine Temperaturverteilung nicht. Die Ausbildung des Temperaturfeldes läuft schneller ab in einer Anlage mit drei Kühlkreisläufen als in einer mit vier Kreisläufen, was auf die reduzierte Wärmekapazität der kompakteren Anlage mit ihrem geringeren Wasservolumen zurückzuführen ist. Versuche mit versperrten Strömungspfaden auf der Primärseite der Zwischenwärmetauscher zeigen, daß das Core dennoch kühlbar bleibt. Kaltes Wasser aus dem Oberplenum dringt von oben in die Kernelemente (Thermosiphon-Effekt) und in die Spalte zwischen den Kernelementkästen ein, die im NEPTUN Modell simuliert sind. Die Temperaturen am oberen Ende des Kerns steigen hierbei nur leicht an. Zur Kühlbarkeit des Kerns trägt das in den Zwischenkastenräumen zirkulierende Fluid erheblich bei.

Das thermohydraulische Rechenprogramm FLUTAN wurde zur drei-dimensionalen Simulation der Mehrzahl der stationären RAMONA und NEPTUN Experimente sowie weniger ausgewählter transienter RAMONA Versuche verwendet. Der Vergleich von numerisch bestimmten Daten mit Meßergebnissen führt zu einer qualitativ und quantitativ zufriedenstellenden Übereinstimmung. Diese Feststellung gilt sowohl für die Isothermenfelder als auch für die Temperaturprofile im Oberplenum und selbst für die sehr komplexe Kerngeometrie der NEPTUN Anlage.

CONTENTS

1. INTRODUCTION

The reliable removal of decay heat after the shutdown of a nuclear reactor is an important safety criterion. For this reason, passive measures are the guiding principle for the design of the European Fast Reactor (EFR) elaborated in a French/British/German cooperation [1], [2], [3].

The investigations into the thermal hydraulics of the passive decay heat removal (DHR) concept were actually initiated in 1984 during the design phase of the former German SNR-2 project. The design of that sodium-cooled pool-type breeder reactor with a thermal power of 3,420 MW_{th} provided the installation of four heat transport loops. Therefore, the primary system consisted of eight intermediate heat exchangers (IHXs) and four primary pumps (PPs). Four independent secondary systems were available each featuring two IHXs. Apart from the normal DHR system via secondary and steam/water circuits, a safety graded passive DHR concept was envisaged which comprised four loops. Each of the loops operating independently from each other was rated to a thermal power of 30 MW_{th} and consisted of a sodium/sodium decay heat exchanger (DHX) immersed in the upper plenum (UP), an intermediate sodium loop, and a sodium/air heat exchanger (AHX) arranged at the bottom end of a stack with air inlet and outlet dampers. Using these direct reactor cooling (DRC) systems, the decay heat can be removed by natural convection on both sodium sides and natural draft on the air side [4], [5], [6]. To enforce the startup of the DRC circuits, the air dampers of the stacks must be opened initiated by an automatic signal of the reactor protection system or in the unlikely case of a complete loss-of-station service power (LOSSP) mechanically by the operator staff.

To prove the inherent safe operation of the DRC systems relying entirely on natural convection, a comprehensive R+D program was performed. For that purpose, the differently scaled test facilities RAMONA and NEPTUN were built basing on the geometrical features of the SNR-2 [7] which are similar to those of the French Superphénix [8]. In 1988, the EFR design work with the realization of three heat transport loops was started. The sodium coolant of this pool-type with a total thermal power of about 3,600 MW_{th} is circulated through the core by three PPs, and the heat is transferred to the secondary sodium by six IHXs. There are six DRC systems which operate independently from each other. The thermal power per unit amounts to 15 MW_{th} under nominal conditions. At that time, the RAMONA setup was almost in operation and the production of the main NEPTUN components was progressing. Therefore, it was decided to go on with the RAMONA-NEPTUN program utilizing four DRC loops, especially as the fundamental thermal hydraulic findings allow comparable insights into the EFR behavior with six DRC loops. The originally planned investigations into the passive DHR was continued and completed by some key experiments performed in the RAMONA III test facility which represents a three-loop arrangement with six DRC loops according to the

actual EFR geometry. The results of all investigations using the RAMONA and NEPTUN setups are described in summary reports [9], [10], [11]. This paper gives an overview on the decay heat removal by natural convection and provides a comparison of RAMONA with NEPTUN results.

2. OBJECTIVES OF THE INVESTIGATIONS

The decay heat removal concept comprises two diverse systems:

1. A nominal DHR system transfers the heat from the IHX secondary sides to the steam generator units during power operation and during operational decay heat removal via the water/steam plant after a reactor shutdown.

2. In unlikely cases of unavailability of the main heat transfer route or a complete LOSSP, the decay will be removed by a safety graded DRC system.

The latter system has to fulfill the following requirements:

- high reliability,
- simple design,
- passive characteristics,
- low costs.

In order to meet the overall reliability for the DHR function, the DRC system should provide a failure probability of 10^{-6} per demand [4].

For the proof of the feasibility of frequent passive DHR operations, the precise knowledge of temperature loadings of the components are needed. Therefore, it has to be shown that all thermal hydraulic phenomena are well understood and can be described adequately for the transition phase from nominal reactor operation under forced convection to DHR operation under natural convection. The detailed investigations within the RAMONA-NEPTUN program on passive decay heat removal address only the primary system, the most important part of the DRC system [12]. This study focuses firstly on the thermal hydraulics prevailing under nominal conditions, that means the geometry of the primary system is intact and all installed DHXs are serviceable. Of particular interest are:

- the effects of a thermal stratification in the UP on the core cooling (RAMONA and NEPTUN tests),
- the thermal hydraulic interaction between the UP and the core, where the effect of the interstitial flow (NEPTUN tests) is of particular importance for the cooling of the core subassemblies (SAs).

In a second step, the influences of non-nominal operating conditions on the behavior of the primary system are investigated under the assumption that:

- all installed DHXs fail to operate on demand and some time elapses between the reactor shutdown and the operation begin of the DHXs,
- the complete failure of half of the installed DHX circuits,
- the flow channels of all IHXs are blocked at their primary sides leading to a disconnection of the fluid flow from the UP to the core inlet side,
- the coastdown characteristics of the PPs as well as of the pumps at the secondary sides of the IHXs differ remarkably from the nominal values.

An essential aim of the experiments is to generate a broad basis to analyse and identify steady state and transient physical processes which must be modeled in computer codes. Their relevance and quality must be ensured to address specific scenarios and to apply experimental data obtained from down-scaled test facilities to full scale nuclear power plant conditions.

3. PROCEDURE OF THE PROGRAM

- Experiments are carried out in scaled test facilities in order to solve the aforementioned requirements. An important issue for the down-scaling of the prototype DHR systems is the fulfillment of the similarity laws.
- The model experiments should give reliable measurements about the relevant temperature and velocity distributions in the primary system. This must be ensured for the normal operation under forced convection as well as for the transition to natural convection after scram up to quasi-steady state conditions.
- For the extrapolation from model experiments to prototypical conditions, a three-dimensional (3D) thermal hydraulic computer code is necessary. Turbulence models (k,ε-models) and temperature dependent fluid property packages (water and sodium) must be implemented in the code.

The sequence of tasks for the realization of the program is:

- availability of reliable measurements performed in the differently scaled water test facilities RAMONA (1:20) and NEPTUN (1:5),
- pretests with original components (core elements, PPs, IHXs, and DHXs) of the setups in order to determine their thermal hydraulic characteristics (pressure drop, heat transfer, etc.),
- fundamental tests to determine the turbulence characteristics necessary for the modeling of forced and buoyancy driven flows.

4. SIMILARITY CONSIDERATIONS

With respect to an extrapolation of findings based on both measurements conducted in scaled test facilities using water as fluid simulant and validated 3D calculations to prototype conditions, the fundamental question on the proper down-scaling procedure arises in order to catch the crucial physical phenomena. In the following, the most important scaling relations are derived and applied to the down-scaling of the pool-type primary system of a sodium-cooled fast reactor.

The performance of scaled model investigations requires the consideration of the following criteria:

- geometrical similarity of the model and the reactor primary vessel with its main components,
- similarity of the main differential equations describing the velocity and temperature fields within the primary vessel,
- similarity of the boundary, initial, and transient conditions.

From the governing conservation equations, dimensionless groups such as the Richardson number (Ri), the Reynolds number (Re), and the Péclet number (Pe) can be deduced which should be identical for both the prototype and the scaled model. In addition, the relative pressure field induced by the core, the PPs, the IHXs, and the DHXs should be similar. A measure for this is the Euler number (Eu).

For steady state and constant properties, the two-dimensional (2D) equations of momentum and energy in Cartesian coordinates read:

momentum equation

$$\rho\left(\frac{\delta u}{\delta \tau}+u\frac{\delta u}{\delta x}+v\frac{\delta u}{\delta y}\right)=-\frac{\delta p}{\delta x}+\nu\cdot\rho\left(\frac{\delta^2 u}{\delta x^2}+\frac{\delta^2 u}{\delta y^2}\right)+g\cdot\beta\cdot\rho\,(\theta-\theta_o) \quad (1)$$

energy equation

$$\rho\cdot c_p\left(\frac{\delta\theta}{\delta\tau}+u\frac{\delta\theta}{\delta x}+v\frac{\delta\theta}{\delta y}\right)=\lambda\left(\frac{\delta^2\theta}{\delta x^2}+\frac{\delta^2\theta}{\delta y^2}\right) \quad (2)$$

The symbols are defined in a separate nomenclature section. Introducing the dimensionless quantities:

$$U=\frac{u}{\nu/L_o};\ V=\frac{v}{\nu/L_o};\ T=\frac{\theta}{\theta_o};\ P=\frac{p}{\rho\cdot u_o^2};\ X=\frac{x}{L_o};\ Y=\frac{y}{L_o};\ t=\frac{\tau}{\tau_o} \quad (3)$$

into the equations (1) and (2) results in

the dimensionless momentum equation

$$\left(\frac{\delta U}{\delta t} + U\frac{\delta U}{\delta X} + V\frac{\delta U}{\delta Y}\right) = -\frac{\delta P}{\delta X} + \frac{1}{Re}\left(\frac{\delta^2 U}{\delta X^2} + \frac{\delta^2 U}{\delta Y^2}\right) + Ri \tag{4}$$

and the dimensionless energy equation

$$\left(\frac{\delta T}{\delta t} + U\frac{\delta T}{\delta X} + V\frac{\delta T}{\delta Y}\right) = \frac{1}{Pe}\left(\frac{\delta^2 T}{\delta X^2} + \frac{\delta^2 T}{\delta Y^2}\right) \tag{5}$$

For the design and the operation of the scaled RAMONA and NEPTUN test facilities, the dimensionless quantities can be defined as follows:

$$\text{Richardson number: } Ri = \frac{\text{buoyancy force}}{\text{inertia force}} = \frac{g \cdot \beta \cdot \Delta T_{UP} \cdot L_{UP}}{u_o^2} \tag{6}$$

$$\text{Reynolds number: } Re = \frac{\text{inertia force}}{\text{friction force}} = \frac{u_o \cdot L_o}{\nu} \tag{7}$$

$$\text{Péclet number: } Pe = \frac{\text{heat transfer by convection}}{\text{heat transfer by conduction}} = \frac{u_o \cdot L_o}{a} \tag{8}$$

$$\text{Euler number: } Eu^+ = \frac{\left(\frac{\text{pressure force}}{\text{inertia force}}\right)_{DHX}}{\left(\frac{\text{pressure force}}{\text{inertia force}}\right)_{core}} = \frac{\Delta p_{DHX}}{\Delta p_{core}} \cdot \frac{u_{core}^{\,2}}{u_{DHX}^{\,2}} \tag{9}$$

For the UP, the quantities and dimensions are summarized in Fig. 1. Eu^+ denotes the ratio of the pressure drops between the DHX and the core for the model and the reactor, respectively, and thus determines the main flow paths in the primary system. In Fig. 2, the ratios of dimensionless groups Ri*, Re*, Pe*, and Eu* are plotted versus the scale of the test facilities:

$$Ri^* = \frac{Ri_M}{Ri_R}; \quad Re^* = \frac{Re_M}{Re_R}; \quad Pe^* = \frac{Pe_M}{Pe_R}; \quad Eu^* = \frac{Eu_M^+}{Eu_R^+} \tag{10}$$

Using water as model fluid, the geometrically similar 1:20 scaled 3D RAMONA test facility gives Ri, Eu, and Pe numbers which are identical to those of the reactor. For the Re number, however, there exists a deviation of up to 10^{-3}. This means that the RAMONA experiments were performed under laminar conditions. Therefore, the 1:5 scaled NEPTUN apparatus was built which diminishes the Re devi-

ation by about one order of magnitude depending on the supplied heating power and consequently on the corresponding physical properties of the fluid. Thus, an extrapolation of NEPTUN results to the prototype conditions seems to be possible.

Basing on these physical phenomena, the design of the test facilities RAMONA and NEPTUN was carried out choosing a one-dimensional (1D) procedure. The pressure losses Δp along the flow paths can be described by:

$$\Delta p_{loss} = \frac{1}{2} \cdot \zeta \cdot \rho \cdot u^2 \tag{11}$$

The friction coefficient ζ is a function of the geometry and the characteristic velocity u itself. The pressure gain due to buoyancy effects is assessed by:

$$\Delta p_{gain} = \rho \cdot \beta \cdot g \cdot \Delta T \cdot L \tag{12}$$

ΔT denotes the temperature change within or along the heat source or sink relative to the UP bulk temperature. L is the relevant distance along which the buoyant up- or downdraft acts. The power Q of the heat source has to be removed by the heat sink according to the expression:

$$Q = \dot{m} \cdot c_p \cdot \Delta T \tag{13}$$

Substituting the mass flow rate $\dot{m}$ by $(u \cdot \rho \cdot A)$ gives:

$$Q = u \cdot \rho \cdot c_p \cdot A \cdot \Delta T \tag{14}$$

For pure natural convection, the balance of the friction and buoyancy forces must satisfy the equation:

$$\Delta p_{loss} = \Delta p_{gain} \tag{15}$$

$$\frac{1}{2} \cdot \zeta \cdot \rho \cdot u^2 = \rho \cdot \beta \cdot g \cdot \Delta T \cdot L \tag{16}$$

Using the equations (14) and (16), the following characteristic correlations for the velocity and the temperature difference can be deduced in an abbreviated way:

$$u = \left(\frac{1}{\rho \cdot c_p} \cdot \frac{Q}{A} \right)^{1/3} \cdot \left(\frac{2 \cdot \beta \cdot g \cdot L}{\zeta} \right)^{1/3} \tag{17}$$

$$\Delta T = \left(\frac{1}{\rho \cdot c_p} \cdot \frac{Q}{A} \right)^{2/3} \cdot \left(\frac{\zeta}{2 \cdot \beta \cdot g \cdot L} \right)^{1/3} \tag{18}$$

The coolant pool mixing occurs predominantly by penetration of the warm fluid coming from the core into the colder fluid stored in the UP. The warm fluid is guided by the lower contour of the above core structure (ACS) and appears as a horizontally spreading quasi-free jet. The penetration depends strongly on the vertical temperature stratification in the UP (ΔT_{UP}) and on the horizontal flow velocity (u_o), see Fig. 1. A characteristic dimensionless group for this flow behavior is the Ri number. In this case, the Ri number is used to link the characteristic control parameters of the heat source and the heat sink:

$$Ri = \frac{g \cdot \beta \cdot \Delta T_{UP} \cdot L_{UP}}{u_o^2} \tag{19}$$

In order to preserve similarity of the overall thermal hydraulic behavior of the UP, it is obvious that the ratio $Ri^* = Ri_M / Ri_R$ must be one. Using equations (17) and (18) and introducing the assumption $Ri^* = 1$, the dimensionless physical behavior of both test facilities can be determined by the following relations:

$$u^* = \left(\frac{2 \cdot \beta^* \cdot Q^*}{\rho^* \cdot c_p^* \cdot \zeta^*} \right)^{1/3} \cdot X^{1/3} \tag{20}$$

$$\Delta T^* = \left(\frac{\zeta^{*1/2} \cdot Q^*}{\sqrt{2} \cdot \rho^* \cdot c_p^* \cdot \beta^{*1/2}} \right)^{2/3} \cdot X^2 \tag{21}$$

The definition of X is given by:

$$\frac{1}{X} = \frac{L_M}{L_R} \tag{22}$$

$$\frac{1}{X^2} = \frac{A_M}{A_R} \tag{23}$$

With reference to the SNR-2 geometry, the scaling factor amounts to $X = 20$ for the RAMONA model and $X = 5$ for the NEPTUN model. Vertical and horizontal cross-sectons of the RAMONA and NEPTUN models together with the main dimensions in millimeter are shown in Figs. 3 and 4, respectively. The photographs of Figs. 5 and 6 illustrate both setups, in addition.

The experimental results of investigations performed under steady state conditions utilizing the RAMONA and NEPTUN test facilities and the corresponding numerical findings are documented in Refs. [13], [14], [15], [16], [17]. The normalized characteristics Ri*, Re*, and Pe* representing a main result of the investigations are plotted versus the dimensionless model power $Q^* = Q_M / Q_R$ in Fig. 7. The symbols indicate findings obtained from experiments carried out in both

test facilities. The result reflects the validity of the derived and applied scaling relations and is encouraging for an extrapolation to prototypical conditions.

To characterize the transient behavior of the RAMONA thermal hydraulics, Re, Pe, Ri, and Eu^+ numbers gained from experimental results together with the findings of 1D calculations concerning the SNR-2 reactor are plotted in Figs. 8 through 11 versus the time after scram [18]. For the analytical consideration, the ATTICA-DYANA computer code [6] was applied. With respect to a proper comparison, the same boundary conditions and relevant parameters were utilized in both cases. $Ri^* = 1$ and the criterion of geometrical similarity were taken into account. The diagrams illustrate typical agreements and deviations, respectively, of the transient profiles. The Pe, Ri, and Eu^+ numbers show a fairly sufficient matching over a time period of 10^4 s. The Re numbers, however, deviate from each other by three orders of magnitude. For the Eu^+ number, the similarity is calculated for the natural convection phase in the UP; up to a time of about 400 s, the UP is strongly influenced by forced convection due to the coastdown of the PPs and the secondary circuits of the IHXs.

5. DESCRIPTION OF THE TEST FACILITIES

The model design was based on the idea to start with a small, simple, and easy-to-handle apparatus and to progress successively in both scale and complexity. Water instead of sodium was preferred in order to make use of available measuring techniques and to allow the visualization of the fluid motion. The main design features of the RAMONA and NEPTUN setups are summarized in Table 1.

5.1 Design of the RAMONA Test Facilities

The RAMONA test facilities simulate the primary system of the reactor on a scale of 1:20. RAMONA I and II are full models (360°) with the arrangement of four heat transfer loops according to the SNR-2 concept. RAMONA III is another full model (360°) including a three-loop arrangement similar to the EFR design. All setups made of plexiglass are characterized by an easy accessibility and a relatively quick exchangeability of the installed components. The vessel contains the entire primary system which includes:

- a core consisting of one controllable central heater rod surrounded by eight individually heatable rings forming eight concentric annular flow channels. The maximum core power amounts to 75 kW.
- an ACS equipped with a permeable and impermeable shell, respectively,
- four velocity controlled PPs,
- eight IHXs with secondary circuits to transport the heat,
- four DHXs with a heat removal circuit each.

Table 1. Design features of the test facilities.

Setup / Component	RAMONA 1:20 scaled 3D test facilities	NEPTUN 1:5 scaled 3D test facility
core	1 heatable rod and 8 heatable rings forming 8 concentric annular flow channels	337 heatable 19 rod bundles representing fuel and storage SAs, 312 unheatable units representing shielding and reflector elements
	max. power of 75 kW	max. power of 1,600 kW
	simulation of the radial power profile	simulation of the radial power profile
	no simulation of the interstitial flow	simulation of the interstitial flow
ACS	permeable shell design impermeable shell design	permeable shell design impermeable shell design
PP	axial pump	hydraulic simulation of the PPs and feedlines by 4 units with external pumping
	4 units (RAMONA I, II) 3 units (RAMONA III)	
IHX	straight-tube-type	hydraulic simulation of the shell side primary coolant flow by 8 units with external heat exchange
	8 units (RAMONA I, II) 6 units (RAMONA III)	
DHX	straight-tube-type U-tube-type hybrid-type	straight-tube-type
	4 units (RAMONA I, II) 6 units (RAMONA III)	4 units

5.2 Instrumentation of the RAMONA Test Facilities

About 250 thermocouples (TCs) installed in all components of interest as well as along measuring traverses serve to record fluid temperatures. Velocities and mass flow rates are measured by means of Laser-Doppler anemometers (LDAs) and inductive flowmeters, respectively. More details are given in Ref. [9].

Please note: All axial dimensions reported here are related to the reference level which is located at the bottom end of the high pressure plenum (see Fig. 3).

5.3 Design of the NEPTUN Test Facility

The NEPTUN water test facility made of stainless steel is a 1:5 scaled 3D apparatus which contains four loops. The main features of NEPTUN are:

- the core designed for a maximum power of 1,600 kW consists of 337 heatable fuel and storage SAs as well as 312 unpowered shielding and reflector elements. The 337 SAs are individually heatable in seven annular groups. Each SA consists of 19 heater rods which are hexagonally arranged in circular shroud tubes simulating hexagonal wrappers of the reactor. The shrouds of the unheated shielding and reflector elements are designed to simulate their hydraulic behavior only. About 220 mm below the top end of the core, a perforated plate is installed to simulate the pad plane which supports the elements at the prescribed wrapper-to-wrapper pitch. The interwrapper spaces are filled with circulating water. In contrast to the RAMONA core design, the very detailed modeling of the NEPTUN core geometry allows the investigation of the thermal hydraulic interaction between the core elements, the interwrapper spaces, and the DHXs immersed into the UP of the primary vessel.
- an ACS equipped with a permeable and impermeable shell, respectively,
- a simplified hydraulic simulation of the PPs and feedlines by four dummies with external pumping,
- a simplified hydraulic simulation of the IHXs by eight dummies with external heat exchange,
- four DHXs with a heat removal circuit each.

5.4 Instrumentation of the NEPTUN Test Facility

The most part of the instrumentation consists of TCs. About 1,200 TCs are available which can be subdivided into two groups:

1. stationary measuring devices installed at various locations of interest within the core, the ACS, the PPs, the IHXs, the DHXs, and the different plena of the vessel,

2. measuring devices being installed on movable supporting systems which allow temperature measurements in the UP at nearly each position of the cylindrical coordinate system.

Please note: All axial dimensions reported here are related to the reference level which is located at the bottom end of the high pressure plenum (see Fig. 4).

The mass flow rates through the core are measured by turbine-type flowmeters installed in the suction lines of the PP simulators. More details are given in Ref. [10].

5.5 Operational Procedure

For the investigation of pure natural circulation, power is supplied to the core of the model and the generated heat is removed by the DHXs exclusively. For studies covering the transition from forced to natural convection, all active components are in operation. The transient behavior of the circuits is modeled by given time functions using process control units. To overcome problems arising due to the simplified secondary circuits with hydraulic simulators for the PPs and IHXs of the NEPTUN apparatus, external auxiliary water circuits are used. Details are reported in Ref. [11].

6. NUMERICAL SIMULATION OF THE EXPERIMENTS

For the numerical simulation of the RAMONA and NEPTUN experiments, the thermal hydraulic computer program FLUTAN [19] is utilized to analyze the combined fluid dynamics and heat transport for 3D, laminar and turbulent, steady state and transient problems. The selection of either rectangular Cartesian or cylindrical coordinates is provided. The program includes physical models for volume porosity, surface permeability, surface heat flux, volumetric heat source, thermal interaction between the immersed structure and the surrounding fluid. Two temperature dependent fluid property packages are presently implemented, i.e., for water and sodium. This basic concept and structure of FLUTAN relies on the COMMIX computer program [20] developed in the U.S.A. by the Argonne National Laboratory (ANL). COMMIX was made available to the Research Center Karlsruhe (FZK) in the frame of cooperation contracts in the fast reactor safety field.

The development works and improvements of the FLUTAN code, contributed by several FZK Departments, consist of the following innovative features and options:

- the full vectorization [21],
- the self optimizing algorithm CRESOR [22] for solving the Poisson equations for energy, pressure, and turbulence using a finite difference numerical tech-

nique. CRESOR is a red/black successive overrelaxation (SOR) method combined with the method of conjugate residuals supported by coarse-mesh rebalancing.

- the supplement of second-order differencing schemes (QUICK and LECUSSO technique) [23] in addition to the first-order upwind differencing method (donor cell method) for treating the convective terms of the momentum and enthalpy equations,
- the two-equation standard turbulence model (k,ε-model). For mixed convection flow and for cases which require a detailed simulation of the turbulent heat flux, a turbulence model for buoyant flow is implemented in the code [24].
- the development and validation of a heat exchanger model [25] to accounting for steady state and transient inlet conditions, i.e., mass flow rate and temperature.
- So far, the FLUTAN program is validated for laminar and turbulent forced convection flows under steady state and transient conditions. The same is true for the laminar natural convection flow under both steady state and transient conditions.

7. TYPICAL COMPUTED VELOCITY AND TEMPERATURE FIELDS

For the simulation of the experiments with the FLUTAN computer program, 90° sectors of the RAMONA and NEPTUN test facilities are modeled by using noding schemes of roughly 15,000 and 20,000 volume cells, respectively. The thermal hydraulic characteristics as heat transfer coefficients and friction factors of the core, SAs, and DHXs are specified for the data input by making use of pretest measurements with the original components of the RAMONA and NEPTUN models [14], [26]. Figures 12 and 13 illustrate the nodalization of the setups with examples of some cross-sections. Figure 14 shows typical RAMONA velocity and temperature fields. The computation bases on steady state natural convection conditions. The core power amounts to 8 kW. The upper plots illustrate the flow paths by way of two vertical sectional planes. On the left-hand side, the cross-section O-A is a cutting across the core and the center of a DHX; on the right-hand side, the cross-section O-B includes the core and the center of an IHX. The reference vector represents a velocity of 2.5 cm/s.

The findings describe two main flow paths in the primary system, namely flow path I and II. Flow path I is obtained under forced and natural convection conditions. The vertically upward flowing water is heated up in the core channels and enters the gap between the core and the impermeable ACS. At the bottom end of the ACS, the warm flow is deflected and forced to flow against the direction of the cold stream coming from the DHXs (countercurrent flow). Water of mixing tem-

perature reaches the UP where the flow is bifurcated. One part of the warm fluid enters the IHXs (flow path I) and circulates via the lower plenum (LP), PPs into the high pressure plenum (HPP) where the fluid enters the core again. The other part of the warm fluid reaches the DHX inlet windows. This flow path II is limited to the UP only. In this case, the warm fluid is led from the UP into the DHXs for heat removal. The increase in density caused by the cooling results in a downward flow. The cold fluid leaves the DHXs at the bottom ends and enters the lowest region of the UP, the cavity. Due to the continuous supply of cold water into the cavity, the fluid stored here is displaced beyond the periphery of the core and mixed with warm fluid leaving the core. Conditionally, the cold fluid penetrates into the gap between the core and the ACS and reaches the centerline of the core. On this way, a stratified flow is established.

The corresponding temperature fields are represented by the plots given in lower part of Fig. 14. The isotherm lines have an interval of 1 K. The computations show a uniform temperature of about 40°C in the lower region of the UP, a small layer of closely spaced isotherms in the horizontal area between the top end of the core and the bottom end of the DHX outlet windows, and above another region with a uniform temperature of about 47°C. The horizontal character of the isotherms indicates the formation of a thermal stratification within which the entire temperature rise of 7 K occurs. The highest fluid temperatures take place in the center of the gap formed by the core and the ACS. With increasing distance from the centerline, the temperatures drop in radial direction mainly due to an increasing mixing effect of the cold water coming from the DHXs and the warm flow exiting from the core. Within the heated portion of the core, the isotherms have an essentially horizontal character.

The FLUTAN computer code is also applied to simulate the combined fluid dynamics and heat transport of steady state NEPTUN experiments. The following discussion addresses again a natural convection investigation performed for a core power of 221 kW. Figure 13 shows the nodalization specified for the data input. The arrangement of the fuel, storage, reflector, and shielding elements together with the modeled interwrapper spaces and the radial power profile determine the degree of the core nodalization in radial direction. An azimuthal noding of the interwrapper spaces is not provided. The volume cells of the SAs are described by porosities and permeabilities. Heat transport between the SA regions and the interwrapper space as well as between the core grid plate (HPP) and the interwrapper space is taken into account.

Figure 15 shows NEPTUN typical velocity and temperature fields. The upper plots illustrate the flow paths with examples of two vertical sectional planes. On the left-hand side, there is a cross-section across the SAs of the core and the center of a DHX. On the right-hand side, the cross-section includes an interwrapper plane of the core and the center of an IHX. The reference vector represents a velocity of

5 cm/s. Compared to the RAMONA velocity field (see Fig. 14), the thermal hydraulic behavior of the UP is essentially the same. Within the interwrapper space of the core (upper cross-section on the right), two vortex flows can be seen, one above and one below the horizontal pad plane indicated by a dashed line. Above the pad plane, cold water coming from the DHXs penetrates into the outermost portion of the interwrapper space and proceeds clockwise guided by the pad plane toward the core centerline. As soon as this interwrapper fluid reaches the upper portion of the core, it mixes with the upward flowing warm fluid leaving the SAs. At the periphery of the core mainly, cold water penetrating into the interwrapper spaces proceeds vertically downward and is drawn on the way to the bottom end of the core to an increasing degree in radial direction toward the core center.

The temperature fields with an isotherm interval of 1 K are represented in the lower part of Fig. 15. The result shown in the left diagram corresponds qualitatively to a great degree to the finding of the previous RAMONA case. The diagram shown on the right illustrates the effects of the fluid circulating in the interwrapper spaces on the field of isotherms. Due to the vortex flow below the pad plane, heat is removed from the core grid plate and the powered central portion of the core. The flow behavior above and below the pad plane causes an extension of the temperature profiles up to the core periphery where a vertical orientation of the isotherms can be observed.

8. STEADY STATE RAMONA AND NEPTUN INVESTIGATIONS

The main parameters which were varied during the course of the steady state RAMONA and NEPTUN experiments are summarized in Table 2. The findings of these tests are described in greater detail in Refs. [9], [10]. From the multitude of the conducted tests, therefore, only such are selected here which illustrate the influences of the ACS shell design and of the number of loops installed in the test facilities RAMONA II and III on the thermal hydraulic behavior. Table 3 contains the parameters of these particular experiments.

8.1 Influence of the ACS Design

The influence of the ACS design on the experimentally and numerically determined isotherm fields is illustrated by Fig. 16 with examples of both a permeable ACS shell (test RA.S1, upper part) and an impermeable one (test RA.S2, lower part). The isotherm lines represented in the plots have an interval of 1 K.

The experimental (left-hand side) and computed (right-hand side) findings of the two RAMONA tests reflect a largely horizontal character of the isotherms in the UP due to a thermal stratification. In the case of a permeable design of the ACS shell (test RA.S1), the stratification is present throughout the entire UP. An impermeable ACS causes a strong temperature stratification with a pronounced tem-

Table 2. Main parameters under considerations during the course of steady state RAMONA and NEPTUN experiments.

Setup / Parameter	RAMONA 1:20 scaled 3D test facilities	NEPTUN 1:5 scaled 3D test facility
core power	1 to 8 kW (8 heating groups)	133 to 221 kW (6, 7 heating groups)
core flow paths via - reflector and storage elements - IHX primary loops	---- blocked, unblocked	unblocked, blocked unblocked, blocked
ACS shell design	permeable, impermeable	permeable, impermeable
DHX design	straight-tube-type, U-tube-type, hybrid-type	straight-tube-type
number of DHXs in operation	4, 2 (RAMONA I, II) 6, 3 (RAMONA III)	4, 2
UP fluid level	normal, lowered	normal, lowered

Table 3. Steady state tests under consideration.

Test No. / Parameter	Core power, kW	Number of heating groups	Design of ACS shell	Number of operated DHXs	Flow path via IHX primary loops	FLUTAN code simulation
RA.S1 [1)]	8	8	permeable	4	unblocked	yes
RA.S2 [1)]	8	8	impermeable	4	unblocked	yes
RA.S3 [2)]	1	8	permeable	6	unblocked	no
RA.S4 [2)]	1	8	impermeable	6	unblocked	no
NE.S1	221	6	permeable	4	unblocked	yes
NE.S2	221	6	impermeable	4	unblocked	yes

[1)] Test performed utilizing the four-loop setup RAMONA II.
[2)] Test performed utilizing the three-loop setup RAMONA III.

perature gradient between the top end of the core and the bottom end of the DHX outlet openings. The highest temperatures occur at the centerline of the setup. The results of the FLUTAN simulations carried out for both experiments are in good agreement with the corresponding measurements.

The computed velocity fields shown in Fig. 17 illustrate the influence of the ACS design on the thermal hydraulic behavior with examples of two sectional planes for the NEPTUN tests NE.S1 and NE.S2. The reference vector represents a velocity of 5 cm/s.

On the left-hand side, the cross-sections are cuttings across the SAs of the core and the center of a DHX. On the right-hand side, the cross-sections are cuttings across the interwrapper space of the core and the center of an IHX. Within the UP, a natural circulation path forms between the core and the DHX. A second flow path is established between the UP and the LP via the IHXs. A permeable design of the ACS shell (test NE.S1, upper part) allows a part of the cold fluid coming from the DHXs to enter the 200 mm high gap between the core and the ACS and to advance up to the centerline of the apparatus. One partial flow of mixing temperature is deflected through the ACS. A second part is forced to move along the perforated bottom plate of the ACS in opposite direction of the flowing-in cold water and ascends parallel to the ACS shell into the UP. Within the interwrapper space, two vortexes exist. The reasons for their formation as well as the flow paths established as a result of an impermeable ACS shell were almost discussed in Chapter 7. Therefore, the computations of test NE.S2 (lower part) are shown without any additional comment.

The influence of the ACS design on the experimentally and numerically determined isotherm fields is illustrated in Fig. 18. The isotherm lines have an interval of 1 K. The results of test NE.S1 are given in the upper part and those of test NE.S2 in the lower one. Comparing the numerical (right side) against the experimental findings (left side), it can be seen that the temperature fields of the UP are generally reasonable predicted. Even for the interwrapper spaces of the core, the agreement is acceptable in view of the fact that the chosen nodalization doesn't simulate the interstitial flow in azimuthal direction (see Fig. 13), a measure which is required with respect to the number of mesh cells and consequently to practical restrictions such as computing time.

8.2 Simulation of the EFR Geometry by the RAMONA III Setup

The EFR geometry with three heat transport loops and six DHXs is simulated by utilizing the RAMONA III test facility. Figure 19 shows the measured isotherm fields of test RA.S3 performed with a permeable design of the ACS shell (upper part) and of test RA.S4 with an impermeable shell (lower part). The results of each test are represented with examples of the cross-sections O-A and O-D (see Fig.

12). The isotherm lines have an interval of 0.5 K. The use of a permeable ACS shell results in a field of isotherms extended over the whole UP as expected. The vertical temperature gradient over the thermal stratification layer is reduced and the maximum temperatures occur at the centerline of the rig. This behavior is similar to the findings of test RA.S1 (see Fig. 16) carried out by utilizing the four-loop setup RAMONA II. The installation of an impermeable ACS shell leads to the almost known layer of closely spaced isotherms (see Fig. 16: test RA.S2).

9. TRANSIENT RAMONA AND NEPTUN INVESTIGATIONS

The transient investigations serve to study the thermal hydraulics prevailing after scram of a reactor during the transition phase from forced to natural circulation up to quasi-steady state conditions [10], [11], [27], [28]. The main parameters which were varied during the course of the transient RAMONA and NEPTUN tests are listed in Table 4.

Table 4. Main parameters under considerations during the course of transient RAMONA and NEPTUN experiments.

Setup / Parameter	RAMONA 1:20 scaled 3D test facilities	NEPTUN 1:5 scaled 3D test facility
core power - before scram - after scram	 30, 75 kW 1, 2, 3, 4, 6, 8 kW	 800, 1100, 1450, 1600 kW 133, 155 kW
core flow paths via reflector and storage elements	—	blocked unblocked
ACS shell design	permeable impermeable	permeable impermeable
PP stop after scram	0, 130, 240, 1200 s	25, 240 s (see Table 1: PP)
number of the operated IHXs	8 (RAMONA I, II) 6 (RAMONA III)	8 (see Table 1: IHX)
IHX turnoff time	15, 240 s	25, 240 s
flow paths via IHX primary loops	unblocked blocked	unblocked blocked
number of the operated DHXs	4, 2 (RAMONA I, II) 6, 3 (RAMONA III)	4, 2
DHX startup time	0, 240, 3000 s	240, 3000 s

9.1 Test Parameters

The transient tests under consideration are given in Table 5. This study focuses firstly on the baseline tests which were conducted under nominal conditions, that means all installed DHXs are serviceable. In a second step, the influences of non-nominal operating conditions on the behavior of the primary system are investigated under the assumption that

- all DHXs installed in RAMONA and NEPTUN, respectively, fail to operate on demand and a period of 3,000 s elapses between scram and operation begin of the DHXs,
- only two of the four DHX circuits grouped in pairs in RAMONA as well as in NEPTUN can be put in operation causing an asymmetrical in-vessel cooling mode,
- the flow channels of all IHXs arranged in the NEPTUN test facility are blocked at their primary sides which results in a disconnection of the fluid flow from the UP to the inlet side of the core.

9.2 Comparison of the Baseline Tests

The RAMONA baseline test RA.T1 and the NEPTUN baseline test NE.T1 were carried out under similar boundary conditions in applying a comparable operational procedure. In both experiments, the power is reduced within a few seconds after initiation of scram. At scram, the power drop of the RAMONA test is about three times higher compared to the NEPTUN experiment. This, however, is of minor influence on the physical characteristics of the primary system. The mass flow rate at the IHX secondary sides drops linearly down to zero very quickly. The operation of the DHXs starts at 240 s after scram. At the secondary side of each DHX installed in the RAMONA rig, a mass flow rate of 6.4 g/s and a inlet temperature of about 25°C are kept constant. The corresponding data of the NEPTUN test are: a mass flow rate of 2.1 kg/s per unit and a temperature of 15°C.

In Fig. 20, the data of the RAMONA test are represented on the left and those of the NEPTUN test on the right. The average core mass flow rates are shown in Fig. 20a. At scram, the flow rates start to decrease continuously, drop down to a minimum value at ~0.5 h after scram, recover then again, and reach approximately constant values at ~1.5 h. It can be seen that the stop of the PPs causes a sharp drop of the mass flow through the RAMONA core. Something similar can not be identified from the transient profile of the NEPTUN test. This different behavior can be explained by the higher pressure gradient being effective in the NEPTUN IHXs which are filled with cold water up to the inlet windows as well as by the less abrupt power ramp at scram. The pronounced mass flow reductions of both tests at 0.5 h after scram are mainly attributed to the following facts:

Table 5. Transient tests under consideration.

Test No. / Parameter	Core power before scram, kW	Core power after scram, kW	Number of heating groups	Design of ACS shell	PP stop after scram, s	Flow path via IHX primary loops	Number of operated DHXs	DHX startup time after scram, s
RA.T1 [2] *baseline*	30	1	8	imperm.	130	unblocked	4	240
RA.T2 [2]	30	1	8	imperm.	130	unblocked	4	3000
RA.T3 [2]	30	1	8	imperm.	130	unblocked	2	240
RA.T4 [1] *benchmark*	30	1	8	perm.	130	unblocked	4	240
RA.T5 [2]	30	1	8	perm.	130	unblocked	4	240
RA.T6 [3]	30	1	8	perm.	130	unblocked	6	240
NE.T1 *baseline*	1450	133	6	imperm.	25	unblocked	4	240
NE.T2	1450	133	6	imperm.	25	unblocked	4	3000
NE.T3	1450	133	6	imperm.	25	unblocked	2	240
NE.T4	1450	133	6	imperm.	25	blocked	4	240

[1] Test performed utilizing the four-loop setup RAMONA I.
[2] Test performed utilizing the four-loop setup RAMONA II.
[3] Test performed utilizing the three-loop setup RAMONA III.

- The cold fluid of the IHXs is completely consumed and warm water of UP temperature enters the IHX inlet openings causing a reduction of its natural convection pressure head.
- As a result of the operation start of the DHXs at 240 s after scram, the cavity of the UP is filled up with cold water and a cold fluid layer (temperature stratification) is developed above the core. That stratification leads to a downward pressure gradient within the core.

To compensate both effects, stronger buoyancy forces have to be established within the core. This is achieved by an increase of the temperature difference within the core. This thermal behavior is going on up to ~0.5 h after scram as demonstrated by the data plotted in Fig. 20b. From that time, the temperature rises of the cores decrease and the core mass flow rates increase. The graphs of Fig. 20b show typical transient temperatures measured at the inlet and outlet side of both cores. The RAMONA data represent averaged temperatures. The NEPTUN measurements are taken from a core element (heating group No. 4) which is placed at a radial distance of 362 mm from the core centerline. The transient temperature profiles recorded at the core outlet sides exhibit considerable temperature drops immediately after scram followed by steep rises of the temperatures. The temperature drops are due to the reduction of the core power and the still operating PPs feeding coolant through the core. After the stop of the PPs, the core temperature differences increase again producing the necessary upward buoyancy forces which counteract the aforementioned effects. At the inlet side of the core, the temperatures increase due to the fact that the cold water of the lower plena is mixed with warm water coming from the upper plena. At about 1 h after scram, these temperature differences reach approximately constant values. From the energy balance results that the core powers and the quantities of decay heat removed by the DHXs are about equal at 4 h after scram.

Temperatures measured at the primary side of the DHX inlet and outlet windows are plotted in Fig. 20c. Up to 240 s after scram, the four DHXs of both setups are not in operation and consequently there exist no temperature differences between their inlet and outlet openings. After the start of the DHXs, the outlet temperatures drop immediately. At about 0.5 h after scram, the temperature differences between the inlet and outlet sides amount to 6 K (test RA.T1) and 10 K (test NE.T1), respectively. These temperature differences remain approximately constant while the core inlet and outlet temperatures decrease slightly until steady state conditions are reached at about 4 h after scram.

The transient thermal behavior of the upper plena is illustrated in Fig. 20d. The data represent the development in time of vertical temperature profiles recorded along measuring traverses. Starting with forced convection at the time of 0 s, uniform temperature profiles are registered. After scram, first of all the lowest parts of the upper plena are affected by cold water flowing out from the cores during the steep temperature drops immediately after scram. After start of the DHX operation, the cooling effects are increased considerably in the cavities and in the UP regions below the bottom end of the ACSs. The top ends of the upper plena, however, remain warm during the first 1,500 s after scram. With increasing time after scram, higher level positions begin to be cooled down to a greater extent reaching constant temperature differences between the top and bottom ends of the upper plena at a time of 15,000 s after scram. Temperature stratifications are formed which take place in the regions between the top ends of the cores and the

outlet windows of the DHXs. The temperature gradients amount to about 3 K in the RAMONA test and 5 K in the NEPTUN test and the vertical temperature profiles remain unchanged by far in time.

The comparison of the characteristic findings of RAMONA test RA.T1 with those of NEPTUN test NE.T1 indicates that similar results were obtained even though differently scaled rigs were utilized for the performance of the experiments. In both tests, the Richardson and Euler numbers are the same. The Péclet and Reynolds numbers differ by roughly one order of magnitude. This means that only locally turbulent flow conditions exist during the transient tests even if they are conducted in the NEPTUN apparatus.

9.3 Delayed DHX Startup Time

The only difference between the baseline tests and the tests RA.T2 as well as NE.T2 is the delayed startup time of the DHXs which are put into operation with a lag of 3,000 s after initiation of scram. The test readings are shown in Fig. 21.

From Fig. 21a, it can be seen that the transient profiles of the core mass flow rate are characterized by a first steep drop immediately after scram, a recovering phase, and a second reduction. The first minimum results from the warm water of the UP entering and heating up the IHXs and the second one from the operation start of the DHXs. In the case as distinguished from the baseline tests RA.T1 and NE.T1 (see Fig. 20a), both events are separated and it can be deduced that the heatup phase of the IHXs lasts ~0.3 h and the flow reduction caused by the DHX operation ~0.5 h. The effect of the 3,000 s delayed startup of the DHX operation becomes clearly visible and causes a very strong and distinct reduction of the mass flow rate through the NEPTUN core. The reason for this behavior is the interstitial flow which contributes remarkably to the heat transport within the core. The removal of heat from the SAs to the interstitial flow diminishes the temperature rises of the fluid inside the SAs and hence the buoyancy forces. As a consequence, the core mass flow rate is reduced to a greater degree compared to the RAMONA test.

These effects are reflected by the core temperatures as well which are given in Fig. 21b. The maximum core outlet temperatures are influenced only to a minor degree by the delayed start of the DHX operation, and a less steep temperature increase is registered at the outlet side of the NEPTUN core. These small increases of the core outlet temperatures are due to the heat capacity of the in-vessel coolant and in the case of the NEPTUN test due to the heat transport to the interstitial flow. At 1.2 h after scram, the temperature differences within the core are high enough to increase strongly the buoyancy forces and hence the core mass flow rates. With the onset of this flow augmentation, the maximum core temperatures start to de-

crease. At about 2 h after scram, the core temperature rise is established and held constant.

The measured DHX inlet and outlet temperatures are plotted in Fig. 21c. The delayed start of the DHXs can be easily identified from the characteristic drop of the outlet temperatures. The temperature differences between the inlet and outlet sides are slightly reduced in time. The fluctuations of the outlet temperatures can be explained by the flow pattern of the cold fluid leaving the DHXs and the warm water accumulated in the UP.

The vertical temperature distributions in the upper plena are represented in Fig. 21d. From these profiles, the delayed startup time of the DHXs becomes clearly visible too. After 3,000 s, the temperatures of the upper part of the UP are increased by about 2 K in the NEPTUN rig. Below the top end of the core, however, the temperatures measured in the NEPTUN cavity are lower than those observed at scram time. This is due to the "cold shock" occurring after scram since the power reduction is reached within a few seconds whereas the rundown of the PPs needs 25 and 130 s, respectively. A comparison of the vertical temperature profiles with the corresponding findings represented in Fig. 20d allows the conclusion that the profiles are basically similar in view of a time shift of 3,000 s.

9.4 Complete Failure of Two Neighboring DHX Circuits

The tests RA.T3 and NE.T3 differ from the baseline tests just by the number of the operable DHX circuits. That means that the same amount of decay heat has to be removed by two DHXs only which comes down to a halving of the active heat transferring surfaces since all other test parameters as well as initial and boundary conditions are kept constant. To remove a twice as high power per DHX, an increase of the driving temperature differences and of the mass flow rates at the primary side of the serviceable DHXs is necessary. Since the DHX inlet temperatures and mass flow rates are the same at the secondary sides, the temperature differences between the inlet and outlet openings of the secondary sides are doubled. Consequently, higher driving temperatures between the primary and secondary sides of the serviceable DHXs appear which cause higher temperatures in the upper plena too. The readings of the experiments RA.T3 and NE.T3 are shown in Fig. 22.

After scram, the core mass flow rates measured in both test facilities (see Fig. 22a) are similar to the measurements recorded during nominal operating conditions with four DHXs being in service (see Fig. 20a).

This is also true for the inlet and outlet temperatures of the cores during the first 0.5 h after initiation of scram (see Fig. 22b). With increasing time after scram,

the inlet and outlet temperatures increase slightly until the states of equilibrium are reached, i.e., when the removed decay heat is identical to the heat input.

Figure 22c shows temperature profiles recorded at the primary sides of the two active DHXs. Compared to the baseline tests, the temperature differences are nearly the same, this means that the higher heat transport is mainly caused by increased mass flow rates through the primary sides of the DHXs.

The time depending vertical temperature distributions in upper plena are shown in Fig. 22d. Within the first 1,000 s after scram, the profiles are very similar to those of the nominal tests with four DHXs being in operation (see Fig. 20d). However, as soon as the two DHXs are in full operation, above all the temperatures measured in the upper part of the UPs differ from the symmetrical load case. This is due to the fact that the steady state conditions are reached at a higher temperature level than in the case of nominal operating conditions. In the upper plena, the temperature level increases slightly afterward and reaches steady state at about 20 h after scram. A comparison with the baseline tests shows that the non-nominal operating conditions lead to higher steady state temperature levels which differ by ~5 K in the RAMONA test and by ~8 K in the NEPTUN test.

9.5 Number of the Installed Heat Transfer Loops

The aim of tests RA.T5 and RA.T6 is to demonstrate the influence of the different number of heat transfer loops arranged in the RAMONA II (four-loop design) and RAMONA III (three-loop design) setups on the transient thermal thermal hydraulic behavior. The results of these tests are represented in Fig. 23. The initial and boundary conditions are comparable; in particular: the power reduction, the rundown of the PPs, and the boundary conditions at the secondary sides of the IHXs and DHXs. The size of the DHX heat transfer surfaces are also the same. The size of the IHX heat transfer surfaces, however, are not identical. The heat transfer surfaces of the six IHXs arranged in RAMONA III amounts to 75% of the surfaces available in RAMONA II with eight IHXs. This deviation is caused by the fact that the IHXs of the RAMONA II rig are utilized again in the RAMONA III setup. That has to be kept in mind when the following results are compared. The comments concern mainly the differences with regard to the number of the installed DHX loops since the general thermal hydraulic behavior doesn' t change from the physical point of view.

After scram, the mass flow rate of the RAMONA III core increases faster compared with the RAMONA II core (see Fig. 23a). This is for the reason that the natural convection pressure head exerted by the six IHXs being in operation in the RAMONA III rig is lower in comparison with that of the eight IHXs available in the RAMONA II. The transient profiles of the core inlet and outlet temperatures are different in the tests under consideration (see Fig. 23b). Before scram, a higher

temperature level is registered in test RA.T6. This behavior has to be attributed to the lower number of IHXs being in operation compared to test RA.T5. Since the core power and the secondary side conditions of the IHXs of both tests are identical, the driving temperature difference between the primary and secondary side of the IHXs has to be higher in order to balance the heat transport. The maxima of the core temperatures are reached earlier in time in the RAMONA III apparatus. This is due to the smaller water volume stored in the vessel and results from higher circulation velocities within the primary system. Therefore, the temperature gradients at the inlet and outlet opening of the DHXs are also higher as shown in Fig. 23c. The temperature distributions in the upper plena are comparable as demonstrated by Fig. 23d. In the RAMONA III test, the characteristic temperature gradient above the core is less pronounced in comparison to the measurements performed in RAMONA II. This is due to the minor fluid volume being stored in the UP of the RAMONA III setup.

9.6 Complete Flow Path Blockage of the IHX Primary Sides

The objective of this investigation is to simulate the thermal hydraulic behavior following a possible break of the hot leg piping system in a top-entry loop-type reactor [29], [30]. For that purpose, the inlet windows at the IHX primary sides are closed in order to block the flow paths between the UP, the LP, and the coolant inlet side of the core. This means that the core is only coolable by fluid penetrating from the UP into the SAs and interwrapper spaces, respectively.

Test NE.T4 is a transient experiment and starts under nominal forced convection conditions and initially opened IHX inlet window. Figure 24 shows FLUTAN computed velocity and temperature fields before scram for cross-section O-B which includes the interwrapper space and an IHX (see Fig. 13). At the top end of the core, strong axial velocities exist characterizing the behavior at the outlet side of the SAs. The fluid motion in the interstitial space, however, is very low or even stagnant water is predicted. This is confirmed by the field of isotherms being highly influenced by the core heating and the temperature rise.

After scram, the IHX windows are closed and the primary flow paths via the IHXs are blocked. The vector plot shown on the right-hand side of Fig. 25 addresses the same cross-section as before and illustrates the situation at 18,000 s after scram. In order to draw comparisons, the corresponding velocity field of the baseline test NE.T1 is given on the left-hand side. At 18,000 s after scram, a time at which the steady state of natural convection is almost reached, a strong clockwise flow circulation takes place in the interwrapper spaces. This flow pattern is more pronounced in test NE.T4 than in test NE.T1 which has to be attributed to the enhanced heat transfer from the core elements to the interstitial flow via the wrapper tubes.

To demonstrate again the important cooling part of the interstitial flow, Fig. 26 illustrates the fields of isotherms on the basis of measured and computed data for both the unblocked and blocked flow paths between the upper and the lower plena. The experimentally and numerically determined temperature fields of the blocked case show that the isotherm lines having an interval of 1 K are tighter and indicate a higher temperature gradient for the interwrapper space compared to the baseline test. Hence the contribution of the interstitial flow on the decay heat removal can be assumed to be enhanced. Mass flow rates locally measured in each SA heating group indicate that in the baseline test NE.T1 about 50% of the core power is removed by the interstitial flow. In test NE.T4, the portion amounts to 60%. This contributions are confirmed by heat balances performed on the basis of the computed values. According to that, the core coolability from above seems to be feasible without any difficulty apart from the fact that temperature level is ~4 K higher at the core outlet side. A comparison of the numerically determined isotherm field against the measurements shows a reasonable agreement of the temperatures within the core region, the interstitial spaces, and the UP.

Figure 27 represents the experimental data of the tests NE.T4 (right side) and NE.T1 (left side). During test NE.T4, the core mass flow rate couldn't be registered because the main flow paths between the UP and the LP are blocked. Figure 27b shows temperature transients recorded at the inlet and outlet side of the core. It can be seen that the maximum temperature rise appears at ~0.25 h after scram and amounts to 20 K for test NE.T4. In test NE.T1, the corresponding value is 16 K. At a time of 4 h after scram, the comparable differences come to 15 K and 10 K, respectively. This increased temperature rise for the blocked case can be explained by the fact that the core elements are cooled by thermosyphon effects, i.e., there exists a circulation of warm water in upward direction and of cold fluid in downward direction. It is obvious that these effects produce a higher pressure loss compared to the nominal flow path via IHXs and PPs. In addition, a cooling effect is caused by the interstitial flow. Cold fluid passes the interwrapper spaces and contributes remarkably to the decay heat removal during both tests under consideration. At the DHX inlet and outlet sides (see Fig. 27c), the transient behavior of the compared tests is very similar. A comparison of the data plotted in Fig. 27d on the right-hand side with those represented on the left indicates that the vertical temperature profiles measured in the UP are very similar at the corresponding points of time. This means that the installation of DHXs in the UP above the core leads to a very effective core coolability even in the case of a flow path blockage via the IHX primary loops.

9.7 Numerical Simulation of a Transient RAMONA Experiment

From the multitude of the performed RAMONA tests, a close-to-reality experiment is selected for a numerical simulation using the FLUTAN computer program. The experiment RA.T4 carried out under reactor typical conditions demonstrates

the thermal hydraulic behavior during the transition from forced to natural convection [31]. At scram, the core power is reduced from 30 to 1 kW. The PPs stop at 130 s after scram. At the IHX secondary sides, the pumps are turned off at 15 s after shutdown. The ACS shell is permeable.

For the simulation of the experiment, the RAMONA test facility is modeled using the 3D network shown in Fig. 12. The number of the volume cells is nearly 15,000. The input data required for the computation take into account all components of the primary system as well as their time depending operational behavior. The calculation covers a time period of 3,600 s, i.e., from steady state forced up to a time at which essentially constant conditions of natural convection are reached. The state of equilibrium between constant decay heat of the core and heat removal by the DHXs is obtained after a long-term period of approximately 20 hours. This stationary state is simulated by a separate computer run.

In Fig. 28, the results of the computations (right side) are compared against the measurements (left side). The calculated values of the mass flow rates and of the temperatures prevailing at the inlet and outlet side of the core as well as in the UP are in good agreement with the experimental findings. The time depending vertical temperature profiles of the UP reflect clearly the effect of the cold water flowing from the DHXs into the cavity and the slow filling of the UP with fluid of mixing temperature. At 20 h after scram, the temperature distribution exhibits a thermal stratification with an axial temperature gradient of about 3 K. These phenomena are well predicted by the computations.

It should be mentioned that the ratio of computing to real time amounted to 400 which is less advantageous for the simulation of a series of RAMONA and especially NEPTUN tests utilizing the latest version of the FLUTAN computer code.

10. SUMMARY AND CONCLUSIONS

Experimental and numerical investigations into the steady state thermal hydraulics, the transition phase from forced to natural convection as well as into the long-term quasi-steady state behavior of the reactor primary system were carried out. The differently scaled 3D test facilities RAMONA (scale 1:20) and NEPTUN (scale 1:5) were utilized with water as the simulant fluid. These setups are similar to the pool-type reactor geometry in order to comply with the requirements of the similarity criteria. Deviations of the characteristic dimensionless Re number, however, must be accepted which influence the velocity field and the mass flow dynamics. Under forced convection condition during the prescram phase, the UP reveals identical temperatures. This is also due to the colder temperatures of the LP. The heat production of the core results in about identical temperatures across the core diameter. After scram, the fluid of the UP experiences a thermal stratification as a result of cold coolant supplied by the IHXs and DHXs. This temperature

stratification is maintained during the postscram phase until steady state conditions are reached.

The start of natural convection is mainly influenced by two effects: the temperature increase at the primary side of the IHXs which leads to a reduction of its natural convection pressure head and the startup time of the DHXs causing a cold fluid layer above the core that counteracts the buoyancy forces of the core.

With examples of selected RAMONA and NEPTUN tests, the influence of nominal and non-nominal operating conditions on the thermal hydraulic behavior of the primary system was investigated. The obtained results of the reported experiments can be summarized as follows:

- The thermal hydraulic findings of the RAMONA and NEPTUN tests are similar. Even the qualitative results are comparable due to the similarity of the chosen boundary, initial, and transient conditions of the corresponding tests.
- The installation of a permeable ACS leads to a thermal stratification which is present throughout the entire UP. An impermeable ACS shell causes a strong temperature stratification with a pronounced axial gradient between the top end of the core and the bottom end of the ACS; in the lower and upper parts of the UP, the temperatures are uniform to a large degree.
- A 3,000 s delayed startup time of the DHXs results in an additional temperature rise in the core elements and in the UP. This slightly higher temperatures do not lead to any doubt about the coolability of the primary system and can be mastered by an optimized startup time of the DHXs.
- An asymmetrical cooling mode due to a complete failure of two neighboring DHX circuits causes a remarkably higher final steady state temperature level of the UP, but doesn't alter the overall temperature distribution.
- The replacement of the four-loop RAMONA II rig by the three-loop RAMONA III setup results in a decrease of the fluid inventory contained in the primary system. The transition from forced to natural circulation is affected by this volume reduction. All transient temperature courses are faster and steady state conditions are reached earlier since the heat capacities are lower. are lower.
- A complete flow path blockage of the IHX primary loops leads to an enhanced cooling effect of the interstitial flow and gives rise to thermosyphon (experiment) or backflow effects (computation) inside the core elements. At the upper end of the core, the temperatures increase slightly, but the core coolability from above is feasible without any difficulty.

- The interstitial flow contributes remarkably to the cooling of the core elements. Up to 60% of the core power is transferred by this effect during the transition phase up to the reaching of steady state conditions.

In order to demonstrate capability of the FLUTAN computer program, analytical predictions were compared against the measurements. The obtained results show that all physical effects observed during the course of the steady state and transient RAMONA and NEPTUN experiments can be numerically simulated. The comparison indicates a qualitatively and quantitatively satisfying agreement of the findings. The capability of that advanced version of FLUTAN is encouraging to provide a qualified tool for the transferability of experimental data to reactor-typical conditions. To achieve this goal, the code was highly improved and carefully validated. The improvements include:

- the full vectorization and implementation of a self optimizing algorithm for solving the Poisson equations,
- the supplement of second-order differencing schemes,
- the development and implementation of new turbulence models for buoyant flows and low Re numbers,
- the development and implementation of a heat exchanger model to accounting for steady state and transient inlet conditions.

The results obtained during the course of the RAMONA - NEPTUN program on passive decay heat removal allow to draw the following conclusions:

- The investigations performed in differently scaled test facilities indicate that the decay heat can be removed from the primary system by means of natural convection. Always flow paths develop which ensure an effective cooling of all regions in the primary system of the reactor models.
- This statement can be transferred to the EFR prototypical conditions since the design and operation of the scaled setups are based on the required similarity criteria.
- The findings indicate that the coolability of the primary system is assured even for operating conditions such as the DHXs fail to start on demand and the recovery needs roughly one hour, only half of the DHX circuits can be put in service, or no coolant reaches the core inlet side via IHXs and PPs caused by a complete flow path blockade of the IHX primary loops.
- The improved and assessed version of the FLUTAN computer program represents a promising tool to transfer results gained from water tests to practical situations within the EFR primary vessel, the individual components, and the total DHR system.

11. NOMENCLATURE

a	thermal diffusivity, m^2/s
A	flow cross-section, m^2
Eu	Euler number (pressure/inertia), dimensionless
c	specific heat, W · s/(kg · K)
g	acceleration of gravity, m/s^2
L	characteristic length, m
$\dot{m}$	mass flow rate, kg/s
p	pressure, N/m^2
Pe	Péclet number (conduction/convection), dimensionless
Q	core power, kW
p	pressure, N/m^2
P	normalized pressure, dimensionless
r	radius, m
Re	Reynolds number (inertia/friction), dimensionless
Ri	Richardson number (buoyancy/inertia), dimensionless
t	normalized time, dimensionless
T	normalized temperature, dimensionless
u	characteristic velocity, m/s
U	normalized velocity, dimensionsless
v	characteristic velocity, m/s
V	normalized velocity, dimensionsless
x	length, m
X	normalized length, dimensionless
	scaling factor, dimensionless
y	length, m
Y	normalized length, dimensionless
z	length, m
β	coefficient of thermal expansion, 1/K
Δp	pressure drop, N/m^2
ΔP	normalized pressure drop, dimensionless
ΔT	temperature difference, K
Δz	length difference, m
$\Delta\phi$	angle difference, deg
ζ	friction coefficient, dimensionless
θ	temperature, °C
λ	heat conductivity, W/(m · K)
ν	kinematic viscosity, m^2/s
ρ	density, kg/m^3
ϕ	angle, deg
τ	Zeit, s

Subscripts

c	core
DHX	decay heat exchanger
M	model
p	pressure
R	reactor
th	thermal
UP	upper plenum

Superscript

*	ratio of model/reactor

Abbreviations

ACS	above core structure
AHX	sodium/air heat exchanger
ANL	Argonne National Laboratory
DHR	decay heat removal
DHX	decay heat exchanger
DRC	direct reactor cooling
EFR	European fast reactor
FZK	Forschungszentrum Karlsruhe
HPP	high pressure plenum
IHX	intermediate heat exchanger
LP	lower or cold plenum
LDA	Laser-Doppler-anemometer
LOSSP	loss-of-station service power
NE.S	NEPTUN steady state test
NE.T	NEPTUN transient test
PP	primary pump
RA.S	RAMONA steady state test
RA.T	RAMONA transient test
SA	subassembly
SNR-2	German design of a sodium-cooled fast reactor
SOR	successive overrelaxation
TC	thermocouple
UP	upper or hot plenum
1D	one-dimensional
2D	two-dimensional
3D	three-dimensional

12. REFERENCES

[1] EFR Associates (eds.): European Fast Reactor, consistent design, concept design specification. EFR Associates, 10 rue Juliette Récamir, BP 3087, F-69398 Lyon, Cédex 03, France, EFR A000/0/0034B, September 1991.

[2] EFR Associates (eds.): European Fast Reactor, concept design specification and justification. EFR Associates, 10 rue Juliette Récamir, BP 3087, F-69398 Lyon, Cédex 03, France, EFR A000/0/0333A, June 1993.

[3] EFR Associates (eds.): European Fast Reactor, the approach to Europe's future need for electricity. EFR Associates, 10 rue Juliette Récamir, BP 3087, F-69398 Lyon, Cédex 03, France, December 1993.

[4] M. Düweke, H.J. Friedrich, F. Hofmann, B. Valentin, and R. Webster: The direct reactor cooling system of the EFR, overview and R&D activities. Proc. of the 1990 Internat. Fast Reactor Safety Meeting, Snowbird, UT, USA, Vol. II, pp. 309-318, August 1990.

[5] M. Köhler and H.J. Friedrich: Das passive Nachwärmeabfuhrsystem des European Fast Reactor, (in German), Fachsitzung: Naturumlaufprobleme zur passiven Nachwärmeabfuhr bei fortschrittlichen Reaktoren. Jahrestagung Kerntechnik '91, Bonn, Germany, Kerntechnische Gesellschaft e.V., Deutsches Atomforum e.V., Bonn: INFORUM 1991, pp. 13-46, May 1991.

[6] C. Essig, M. Düweke, V. Ruland, V. Ertel, and M. Kiera: Consistent thermal hydraulic approach of EFR decay heat removal by natural convection. Proc. of the 5th Internat. Topical Meeting on Nuclear Reactor Thermal Hydraulics (NURETH-5), Salt Lake City, UT, USA, Vol. II, pp. 135-142, September 1992.

[7] SNR-2, - Abschlußbericht der SNR-2-Pool-Vorplanung (Phase 1c) (in German), Kraftwerk Union AG, Interatom, Bensberg, No. 41.07117, December 1983.

[8] H. Hoffmann, P. Sardin, and R. Webster: The European R&D program on natural convection decay heat removal of the EFR. Proc. of the Internat. Conf. on Fast Reactors and Related Fuel Cycles, Kyoto, Japan, Vol. II, pp. 13.5/1-5/9, November 1991.

[9] H. Hoffmann, K. Marten, D. Weinberg, H.H. Frey, K. Rust, Y. Ieda, H. Kamide, H. Ohshima, and H. Ohira: Summary report of RAMONA investigations into passive decay heat removal. Forschungszentrum Karlsruhe, Wissenschaftliche Berichte, FZKA-5592, July 1995.

[10] K. Rust, D. Weinberg, H. Hoffmann, H.H. Frey, W. Baumann, K. Hain, W. Leiling, H. Hayafune, and H. Ohira: Summary report of NEPTUN investiga-

tions into the steady state thermal hydraulics of the passive decay heat removal. Forschungszentrum Karlsruhe, Wissenschaftliche Berichte, FZKA-5665, December 1995.

[11] D. Weinberg, H. Hoffmann, K. Rust, H.H. Frey, K. Hain, W. Leiling, and H. Hayafune: Summary report of NEPTUN investigations into the transient thermal hydraulics of the passive decay heat removal. Forschungszentrum Karlsruhe, Wissenschaftliche Berichte, FZKA-5666, December 1995.

[12] D. Weinberg, H. Hoffmann, K. Hain, F. Hofmann, and M. Düweke: Experimental and theoretical program to study the natural convection decay heat removal system of the SNR-2. Proc. of the Internat. Conf. on Science and Technology of Fast Reactor Safety, St. Peter Port, Guernsey, Great Britain, Vol. 1, pp. 289-294, May 1986.

[13] H. Hoffmann and D. Weinberg: Investigations on natural convection decay heat removal for the EFR using various model geometries. Proc. of the Internat. Conf. on Design and Safety of Advanced Nuclear Power plants. Tokyo, Japan, Vol. III, pp. 26.2/1-2/7, October 1992.

[14] H. Hoffmann, D. Weinberg, W. Baumann, K. Hain, W. Leiling, K. Marten, H. Ohira, G. Schnetgöke, and K. Thomauske: Scaled model studies of decay heat removal by natural convection for the European fast reactor. M. Courtaud and J.M. Delhaye (eds.): Proc. of the 6th Internat. Topical Meeting on Nuclear Reactor Thermal Hydraulics (NURETH-6), Grenoble, France, Vol. 1, pp. 54-62, October 1993.

[15] H. Hoffmann, K. Hain, H. Hayafune, K. Marten, K. Rust, and D. Weinberg: Experimental studies on passive decay heat removal by natural convection under nominal and non-nominal conditions. F.B. Cheung and E.V. McAssey (eds.): Natural circulation phenomena in nuclear reactor systems. Papers presented at the 1994 Internat. Mechanical Engineering Congress and Exposition, Chicago, IL, USA, HTD-Vol. 281, pp. 1-9, November 1994.

[16] D. Weinberg, K. Rust, H. Hoffmann, H. Hayafune, and H.H. Frey: Comparison of code predictions against natural convection experiments. F.B. Cheung and E.V. McAssey (eds.): Natural circulation phenomena in nuclear reactor systems. Papers presented at the 1994 Internat. Mechanical Engineering Congress and Exposition, Chicago, IL, USA, HTD-Vol. 281, pp. 11-21, November 1994.

[17] D. Weinberg, H. Hoffmann, and K. Rust: Experimental investigations and numerical simulations of three-dimensional temperature and velocity fields in the transition region from laminar forced to natural convection. G.F.

Hewitt (ed.): Heat transfer 1994. Proc. of the 10th Internat. Conf., Brighton, Great Britain, Vol. 5, pp. 585-590, August 1994.

[18] D. Weinberg, D. Suckow, U. Müller, and H. Hoffmann: The transferability of thermal hydraulic model investigations into decay heat removal to reactor conditions. Proc. of the ANS Internat. Fast Reactor Safety Meeting, Snowbird, UT, USA, Vol. 2, pp. 341-350, August 1990.

[19] H. Borgwaldt, W. Baumann, and G. Willerding: FLUTAN input specifications. Kernforschungszentrum Karlsruhe, KFK-5010, May 1992.

[20] H.M. Domanus, W.T. Sha, R.C. Schmitt, V.L. Shah, F.F. Chen, and C.C. Miao: COMMIX-1B: A three-dimensional transient single-phase computer program for thermal hydraulic analysis of single- and multi-component systems; Volume I: Equations and numerics; Volume II: Users manual. NUREG/CR-4348, ANL-85-42, September 1985.

[21] H. Borgwaldt and H.H. Frey: Vektorisierung und Einsatz eines 3D-Thermohydraulik Codes auf dem Siemens Vektorrechner VP50 (in German). A. Schreiner (ed.): Tagungsband anläßlich des Symposiums zur Vorstellung des Projektes ODIN und zur Inbetriebnahme des des Höchstleistungsrechners Siemens VP400-EX. Technische Universität Karlsruhe, Germany, pp. 59-72, April 1989.

[22] H. Borgwaldt: CRESOR, - A robust vectorized Poisson solver implemented in the thermal hydraulic Code COMMIX-2(V). Proc. of the First Internat. Conf. on Supercomputing in Nuclear Applications, Mito City, Japan, pp. 346-351, March 1990.

[23] K. Sakai and D. Weinberg: Investigation on the LECUSSO (locally exact consistent upwind scheme of second order) scheme, - Extension to nonuniform mesh size grids and numerical stability analysis, application for natural circulation test analyses using COMMIX-2(V). Proc. of the First Internat. Conf. on Supercomputing in Nuclear Applications, Mito City, Japan, pp. 57-62, March 1990.

[24] L.N. Carteciano: Entwicklung eines Turbulenzmodells für Auftriebsströmungen (in German). PhD Thesis, Technische Universität Karlsruhe, Germany, April 1996.

[25] A. Class: unpublished internal report, January 1990.

[26] H. Hoffmann, K. Marten, D. Weinberg, Y. Ieda, and H.H. Frey: Investigations of inherent decay heat removal performances in LMFBRs. Proc. of the In-

ternat. Meeting on the Safety of Next Generation Power Reactors, Seattle, WA, USA, pp. 830-837, May 1988.

[27] H. Hoffmann, K. Marten, D. Weinberg, and H. Kamide: Thermal hydraulic model experiments on the transition from forced to natural circulation for pool-type fast reactors. Nuclear Technology, 99, pp. 789-793, 1990.

[28] D. Weinberg, K. Rust, H. Hoffmann, H. Hayafune, and K. Hain: Transient NEPTUN experiments on passive decay heat removal. Proc. of the 3rd JSME/ ASME Joint Internat. Conf. on Nuclear Engineering (ICONE-3), Kyoto, Japan, Vol. 1, pp. 519-524, April 1995.

[29] Y. Eguchi, K. Yamamoto, T. Funada, T. Koga, H. Takeda, K. Sasaki, H. Kajiwara, M. Toda, and I. Maekawa: Experimental and computational study on prediction of natural circulation in top-entry loop-type FBR. Proc. of the Specialists' Meeting on Evaluation of Decay Heat Removal by Natural Convection, O-arai, Japan, IWGFR/88, pp. 86-96, February 1993.

[30] T. Koga, H. Takeda, S. Moriya, T. Funada, K. Yamamoto, Y. Eguchi, K. Sasaki, H. Kajiwara, O. Watanabe, and I. Maekawa: Natural circulation water tests for top-entry loop-type LMFBR. M. Courtaud and J.M. Delhaye (eds.): Proc. of the 6th Internat. Topical Meeting on Nuclear Reactor Thermal Hydraulics (NURETH-6), Grenoble, France, Vol. 2, pp. 1302-1308, October 1993.

[31] D. Weinberg, H.H. Frey, and H. Tschöke: A three-dimensional transient calculation for the reactor model RAMONA using the COMMIX-2(V) code. H. Küsters (ed.): Proc. of the Joint Internat. Conf. on Mathematical Methods and Supercomputing in Nuclear Applications, Vol. 1, pp. 292-303, Karlsruhe, Germany, April 1993.

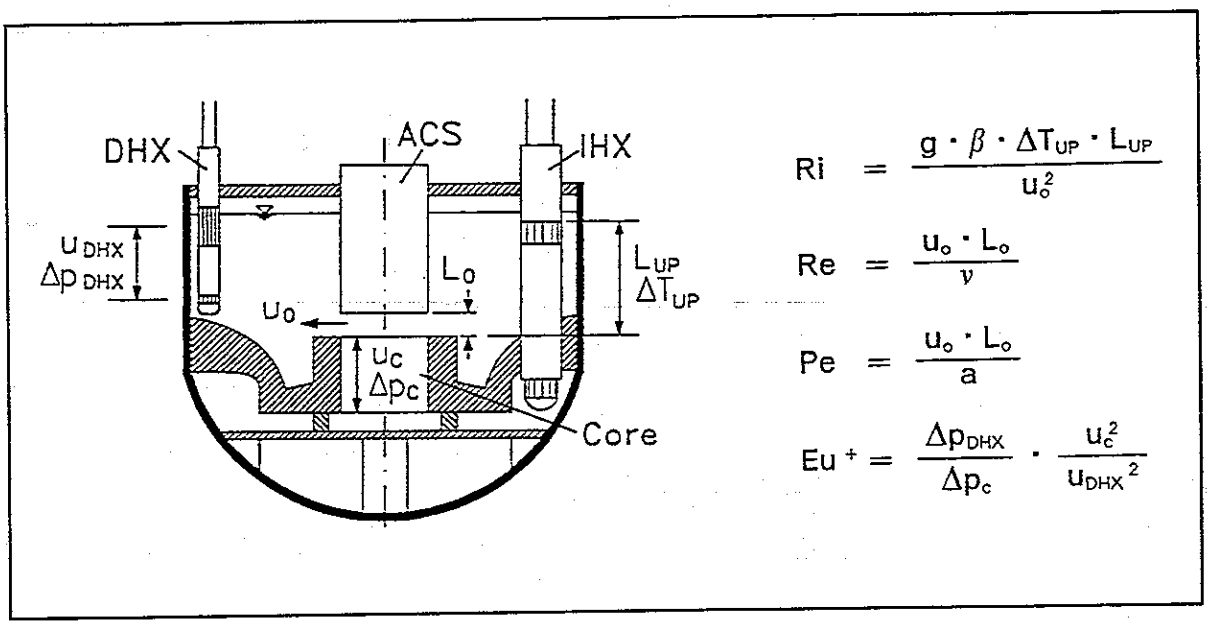

Fig. 1. Definition of the characteristic numbers.

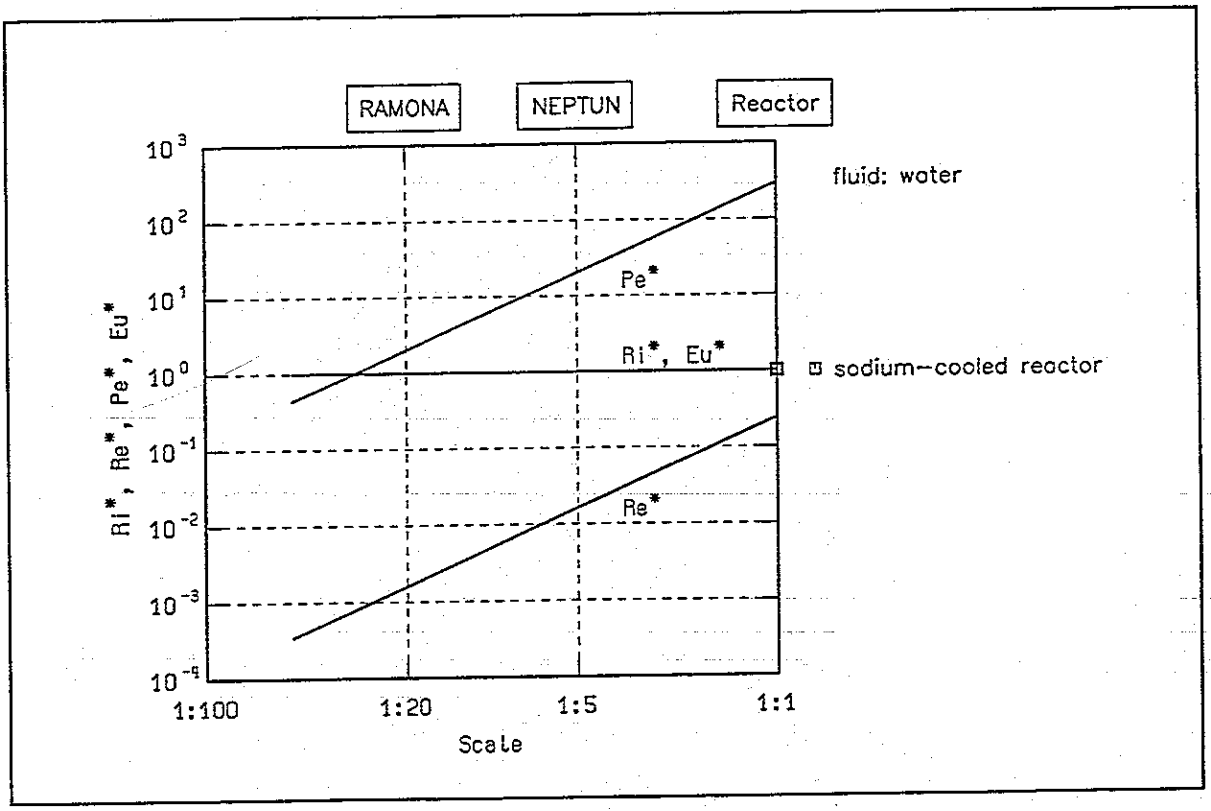

Fig. 2. Characteristic numbers as function of the model scale.

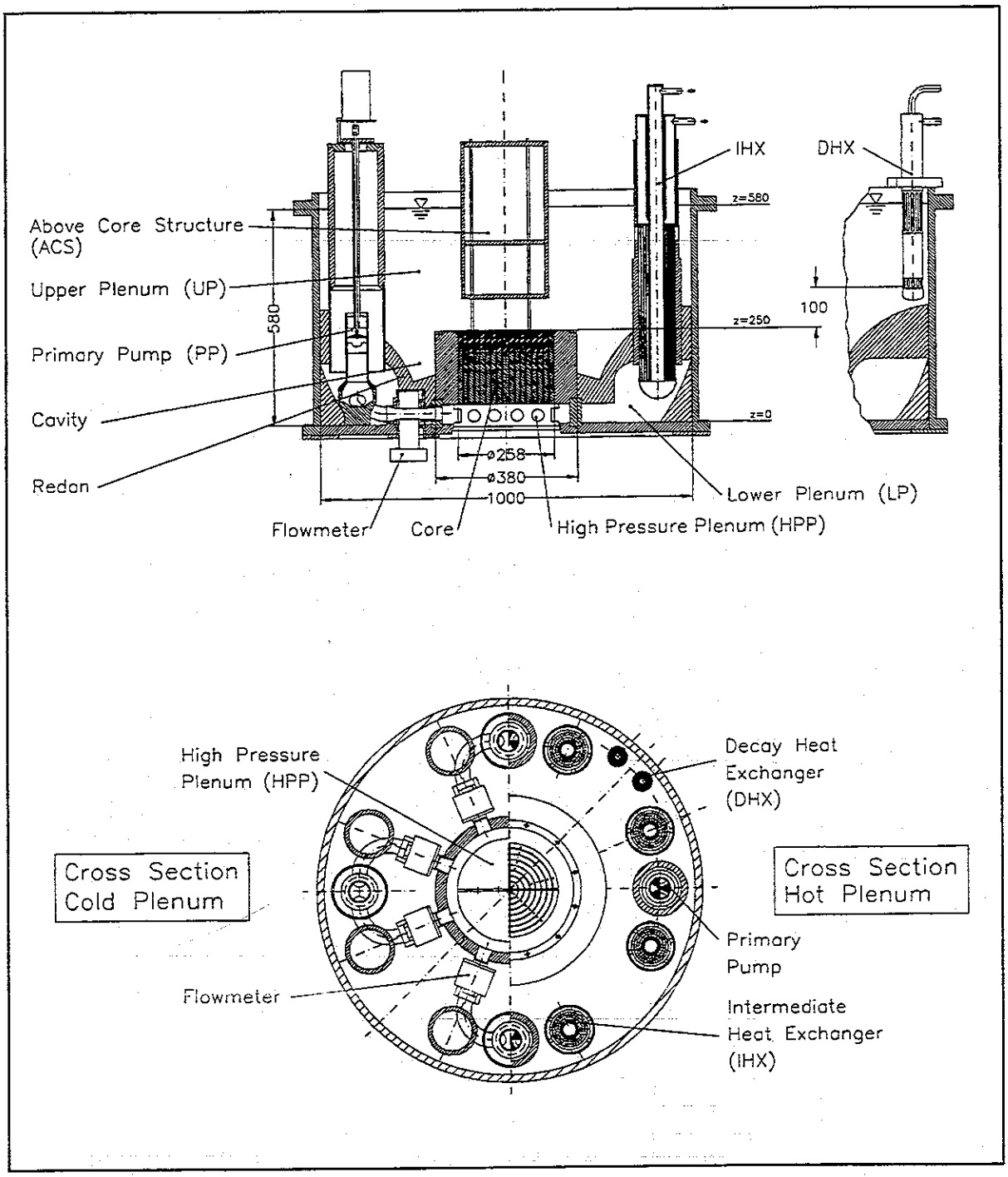

Fig. 3. Vertical and horizontal cross-sections of the RAMONA II test facility (dimensions in millimeter).

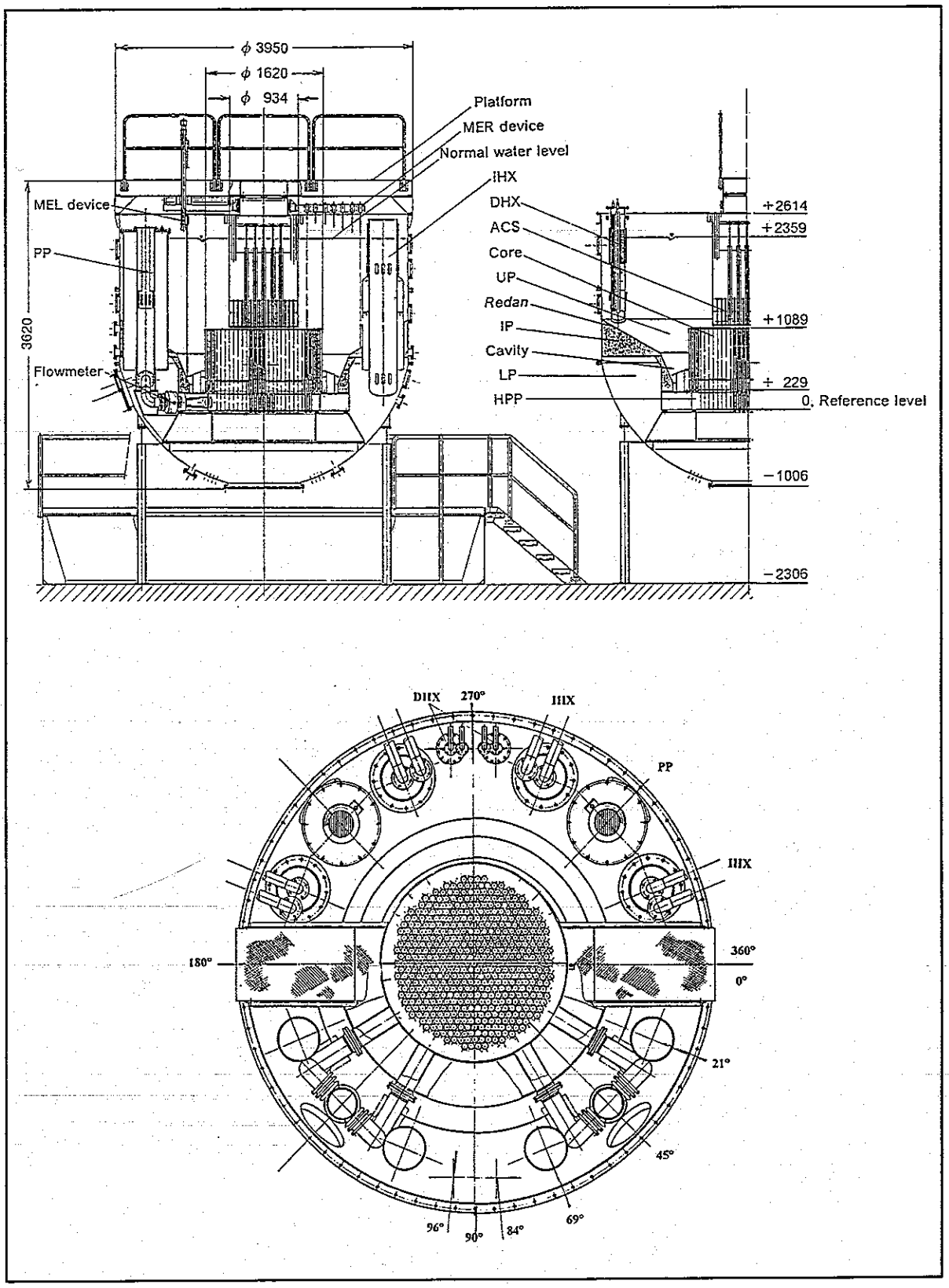

Fig. 4. Vertical and horizontal cross-sections of the NEPTUN test facility (dimensions in millimeter).

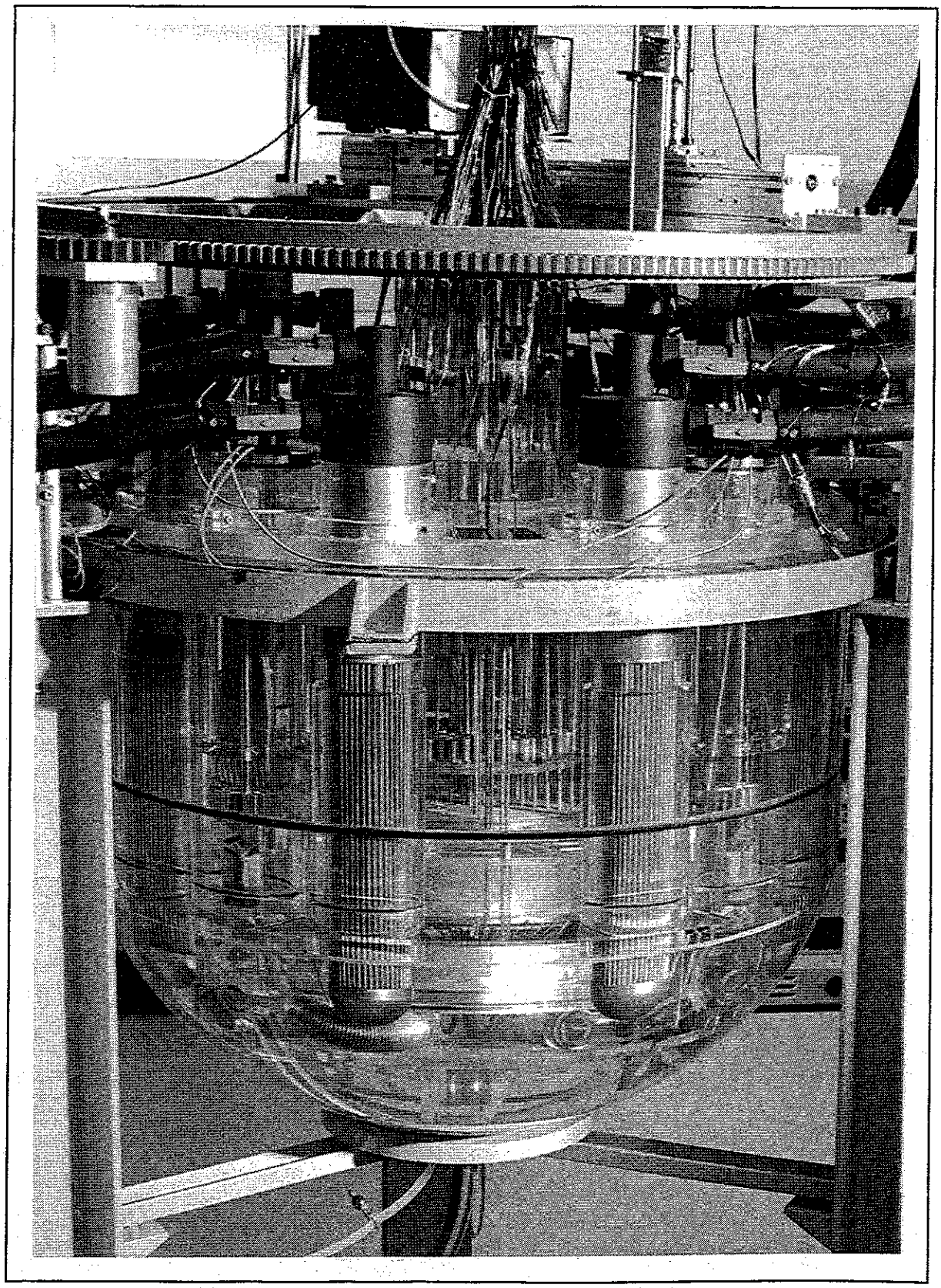

Fig. 5. Side view of the RAMONA test facility.

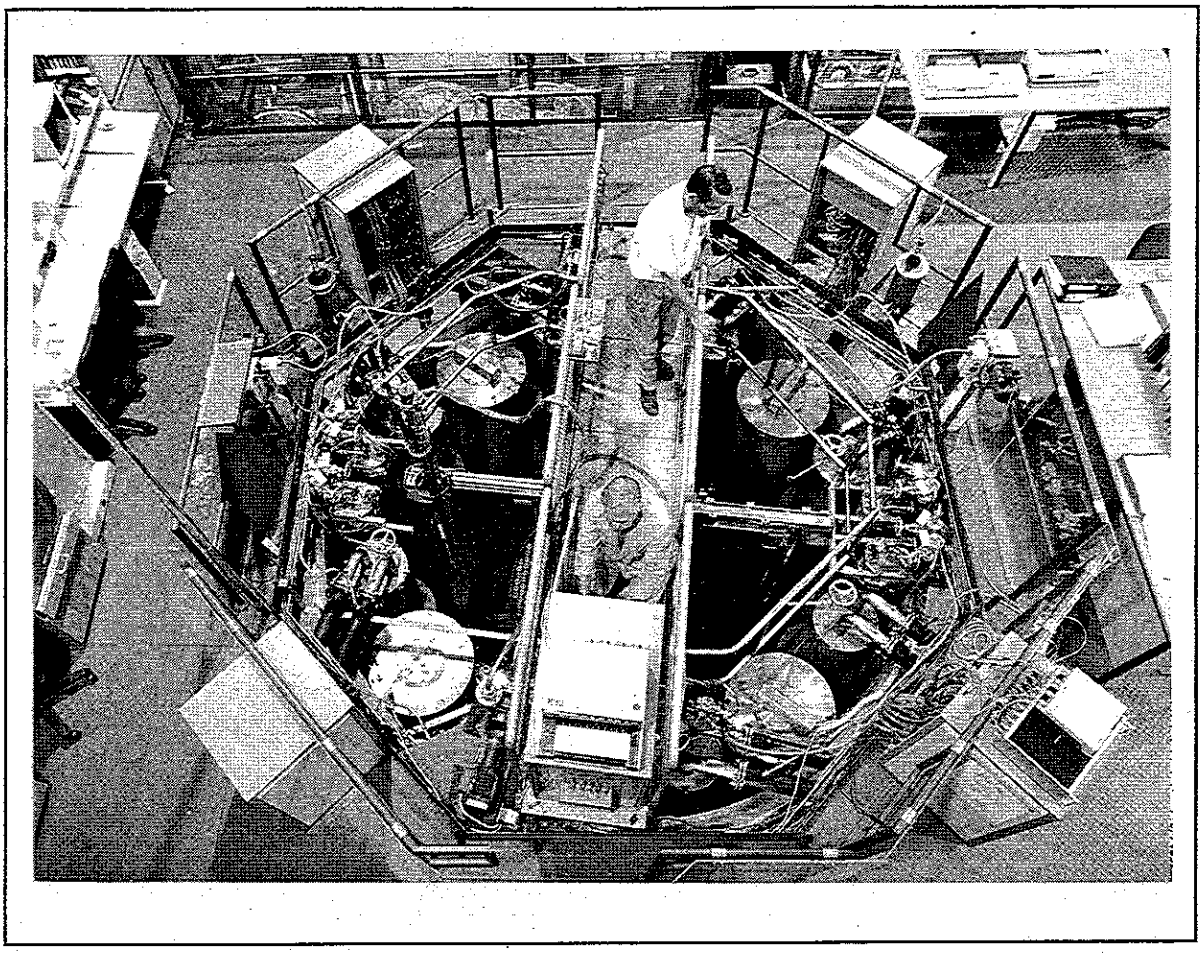

Fig. 6. Bird's eye view of the NEPTUN test facility equipped for the performance of the transient experiments.

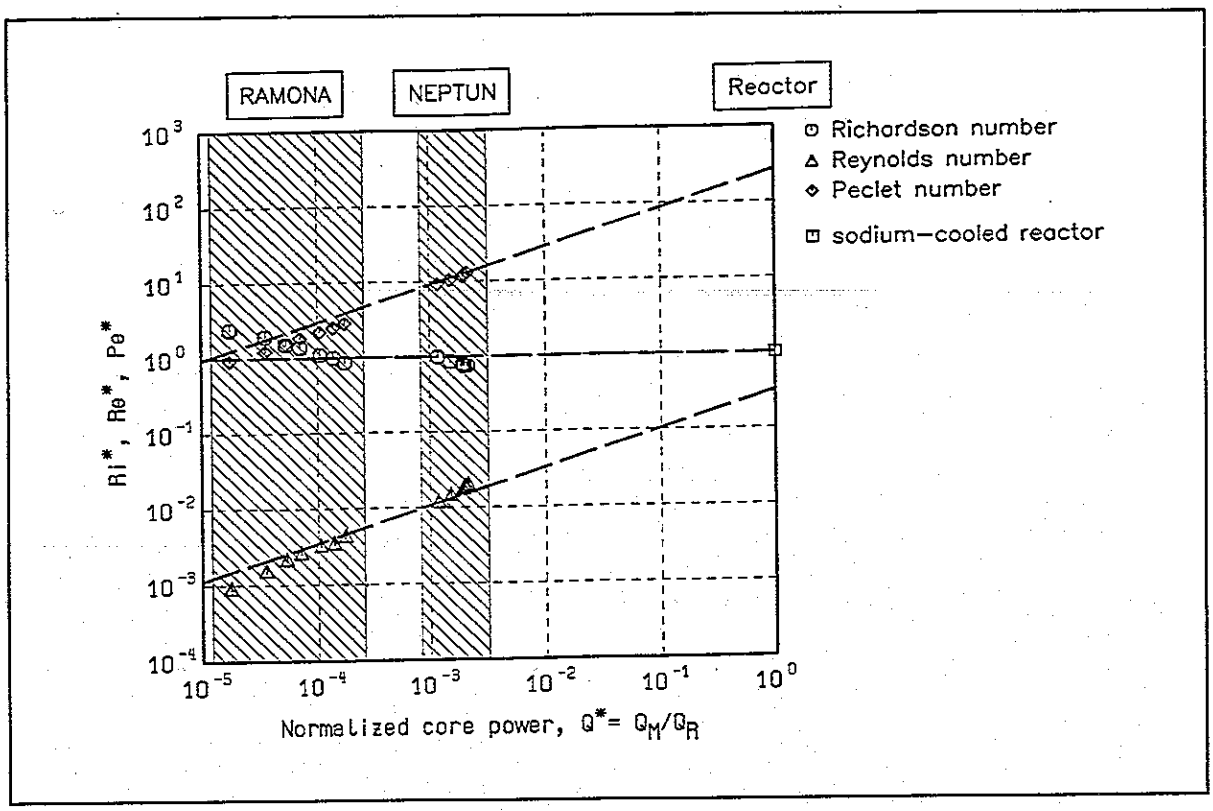

Fig. 7. Characteristic numbers as function of the normalized power.

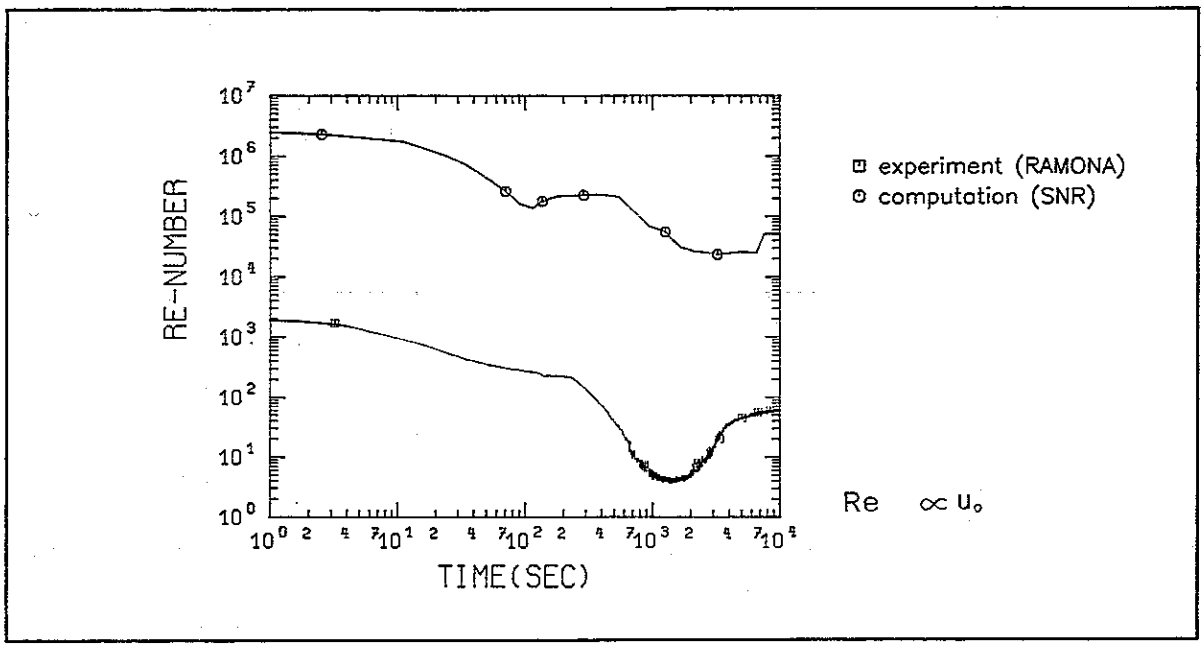

Fig. 8. Comparison of experimentally and numerically determined Reynolds numbers as function of the time after scram.

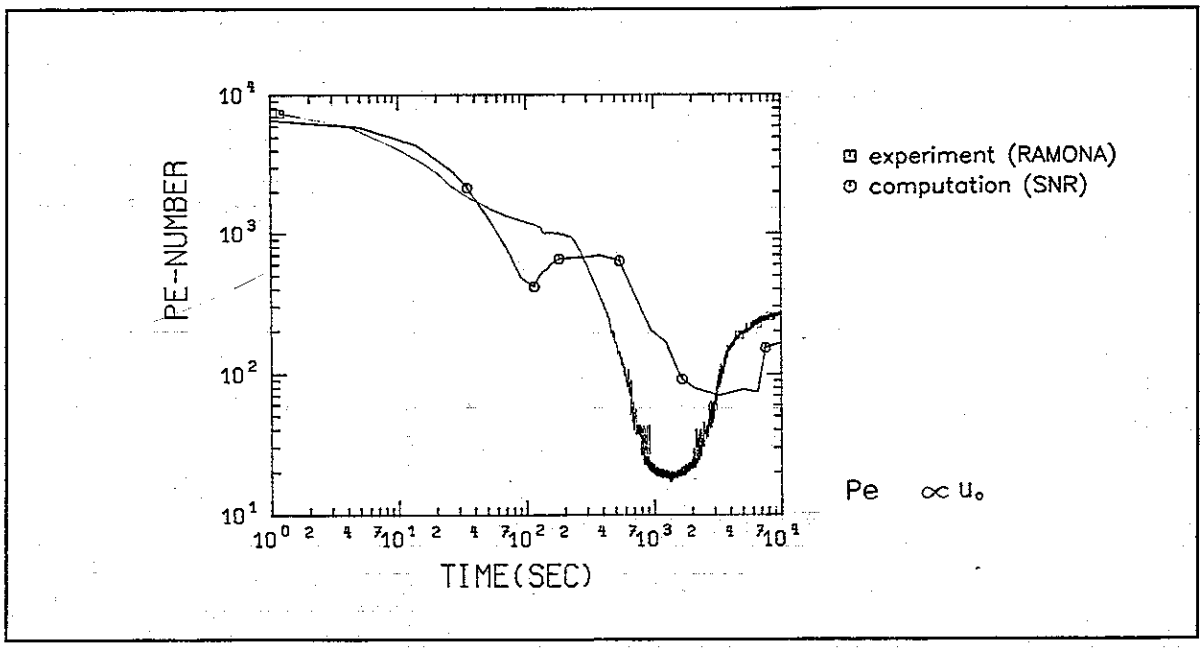

Fig. 9. Comparison of experimentally and numerically determined Péclet numbers as function of the time after scram.

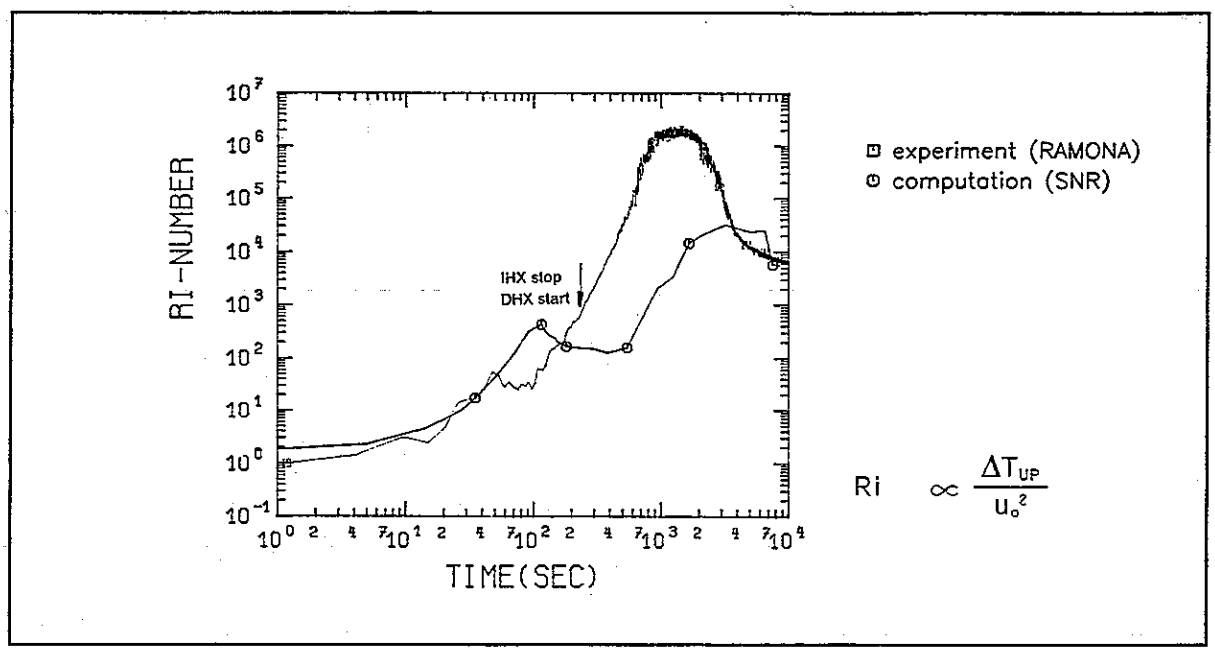

Fig. 10. Comparison of experimentally and numerically determined Richardson numbers as function of the time after scram.

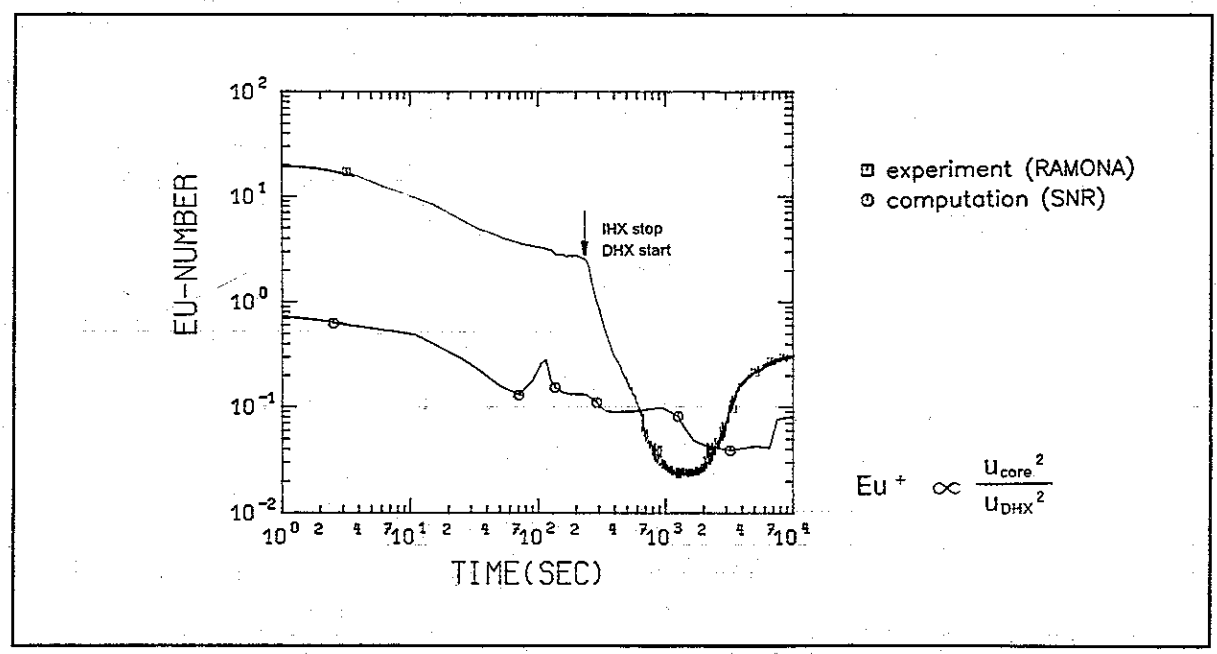

Fig. 11. Comparison of experimentally and numerically determined Euler numbers as function of the time after scram.

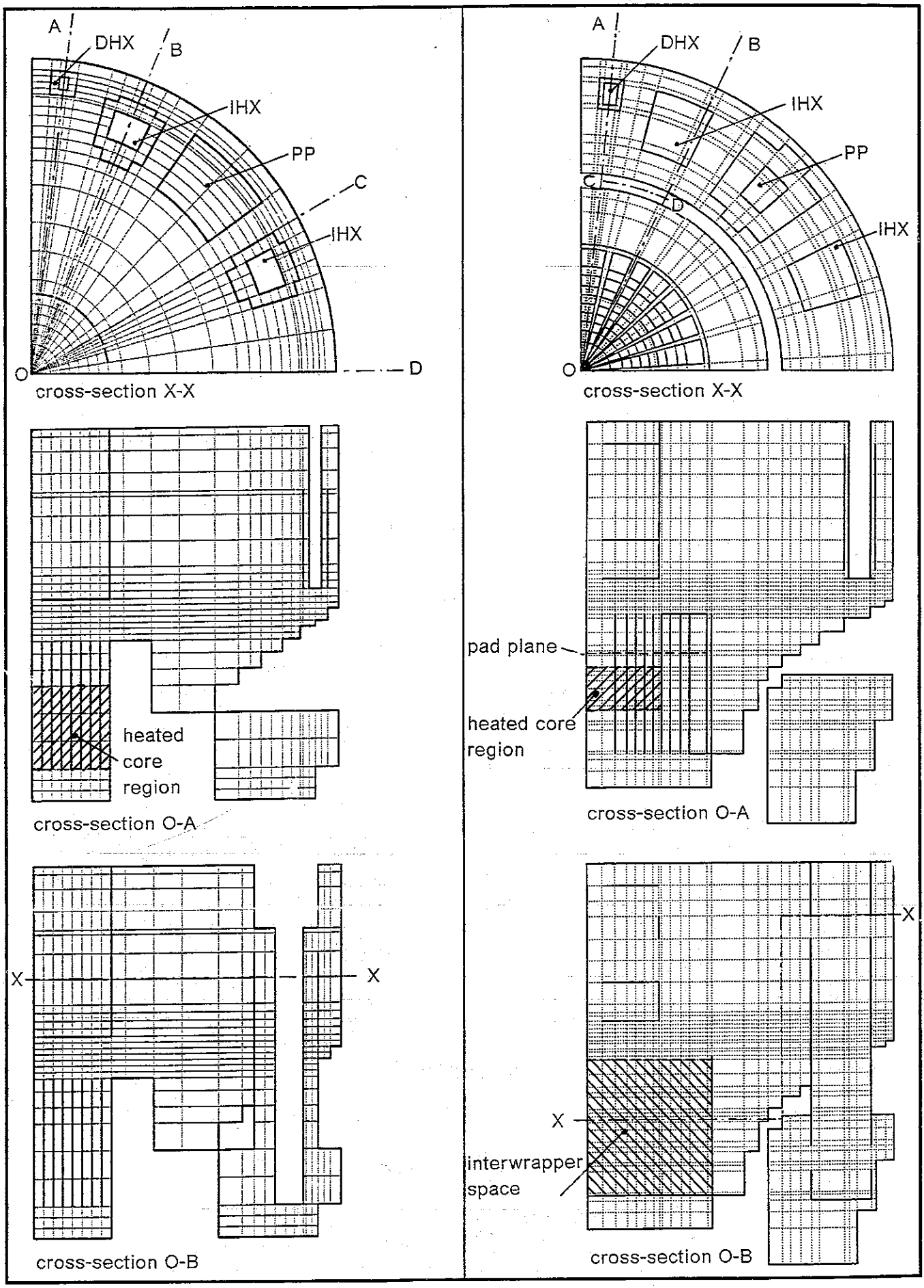

Fig. 12. Nodalization of the RAMONA rig.

Fig. 13. Nodalization of the NEPTUN rig.

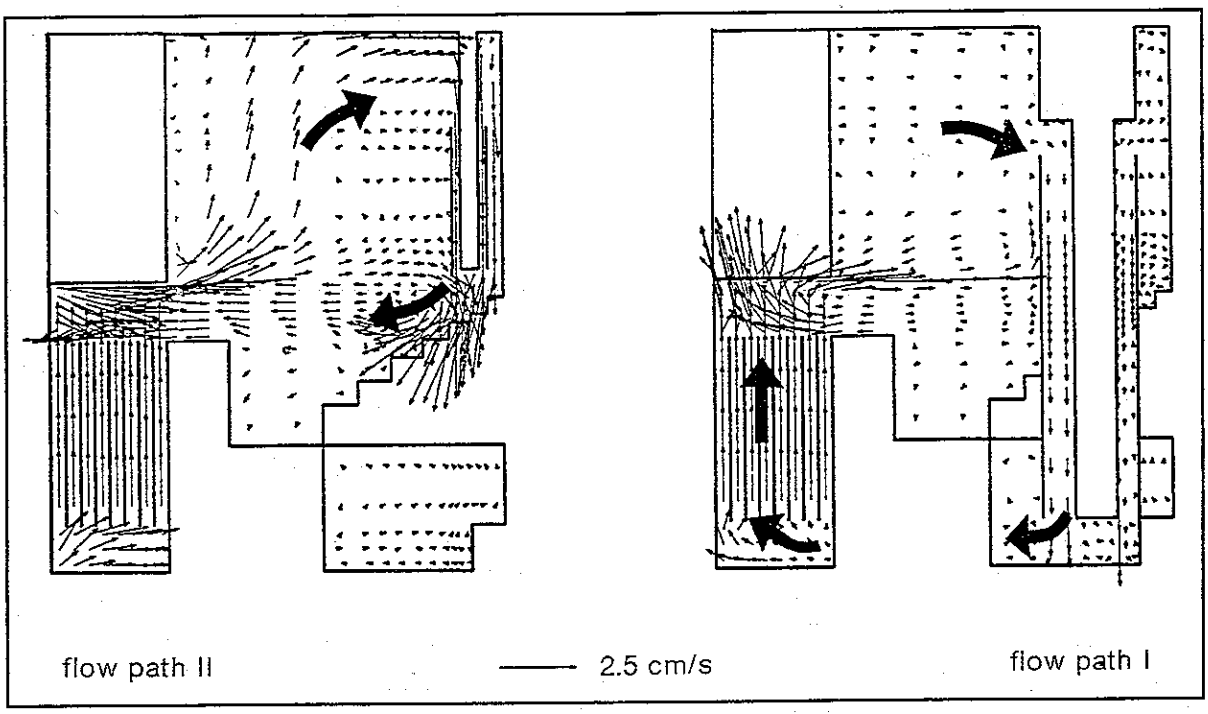

a) Velocity fields and flow paths.

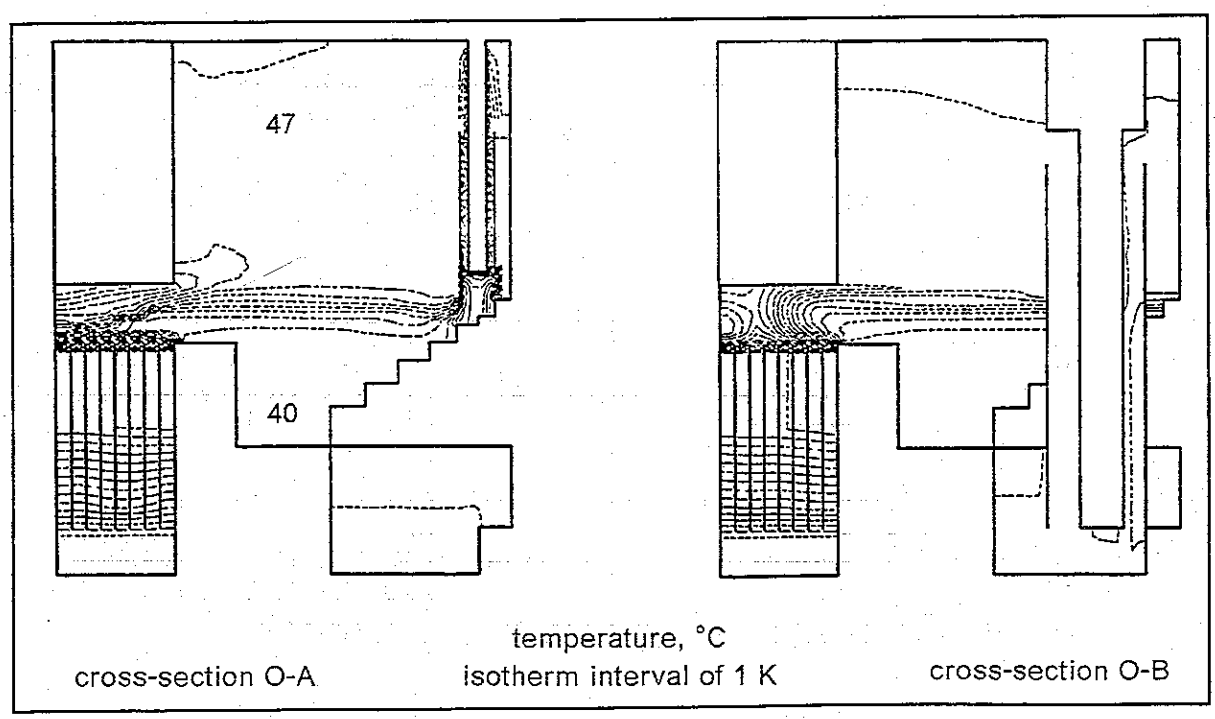

b) Isotherm fields.

Fig. 14. Typical computed velocity and isotherm fields of a steady state RAMONA test.

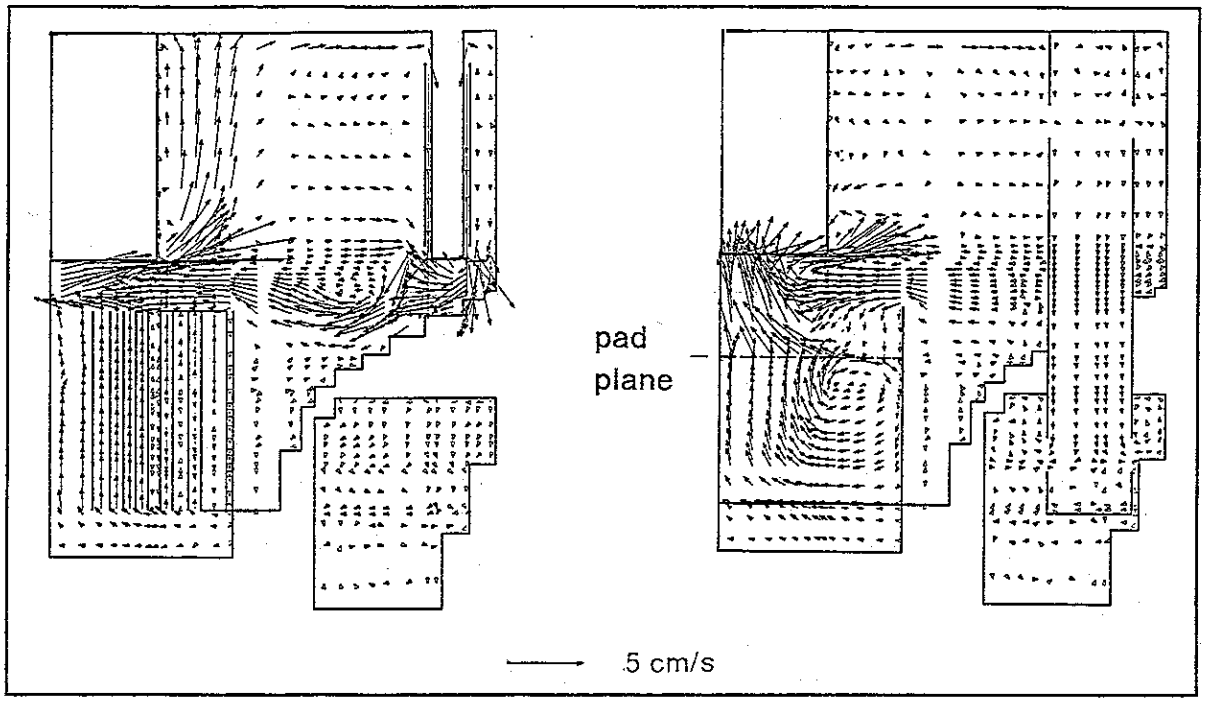

a) Velocity fields.

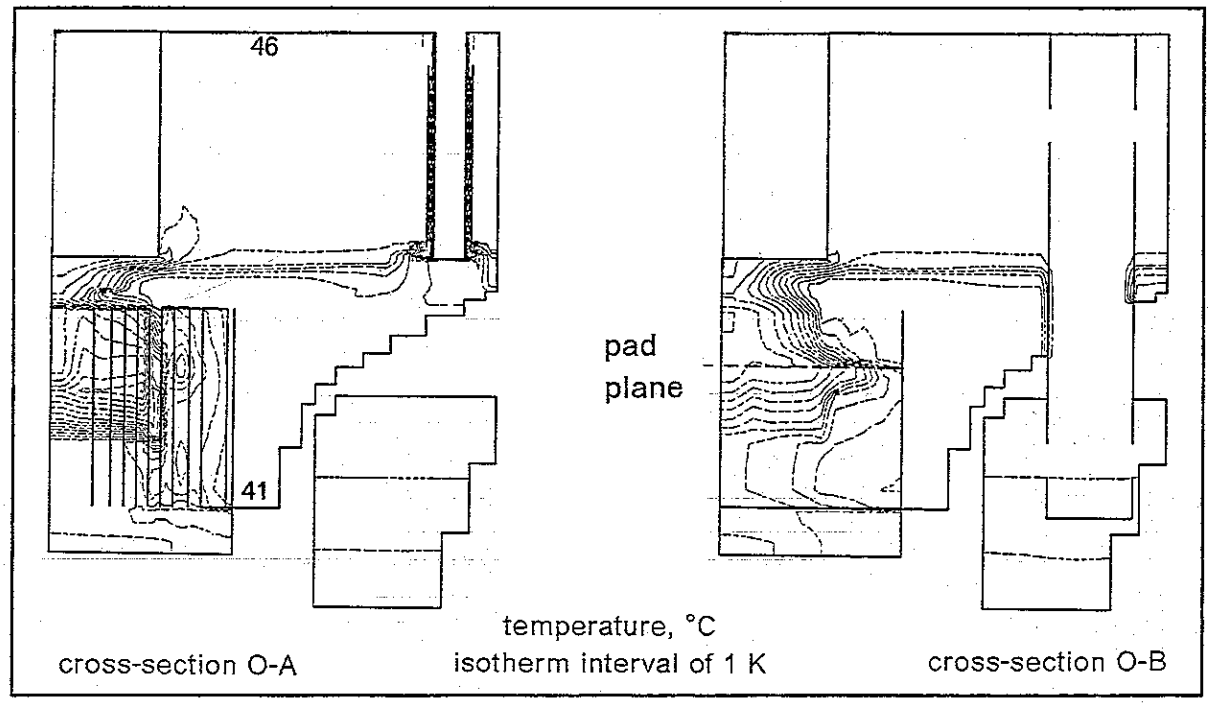

b) Isotherm fields.

Fig. 15. Typical computed velocity and isotherm fields of a steady state NEPTUN test.

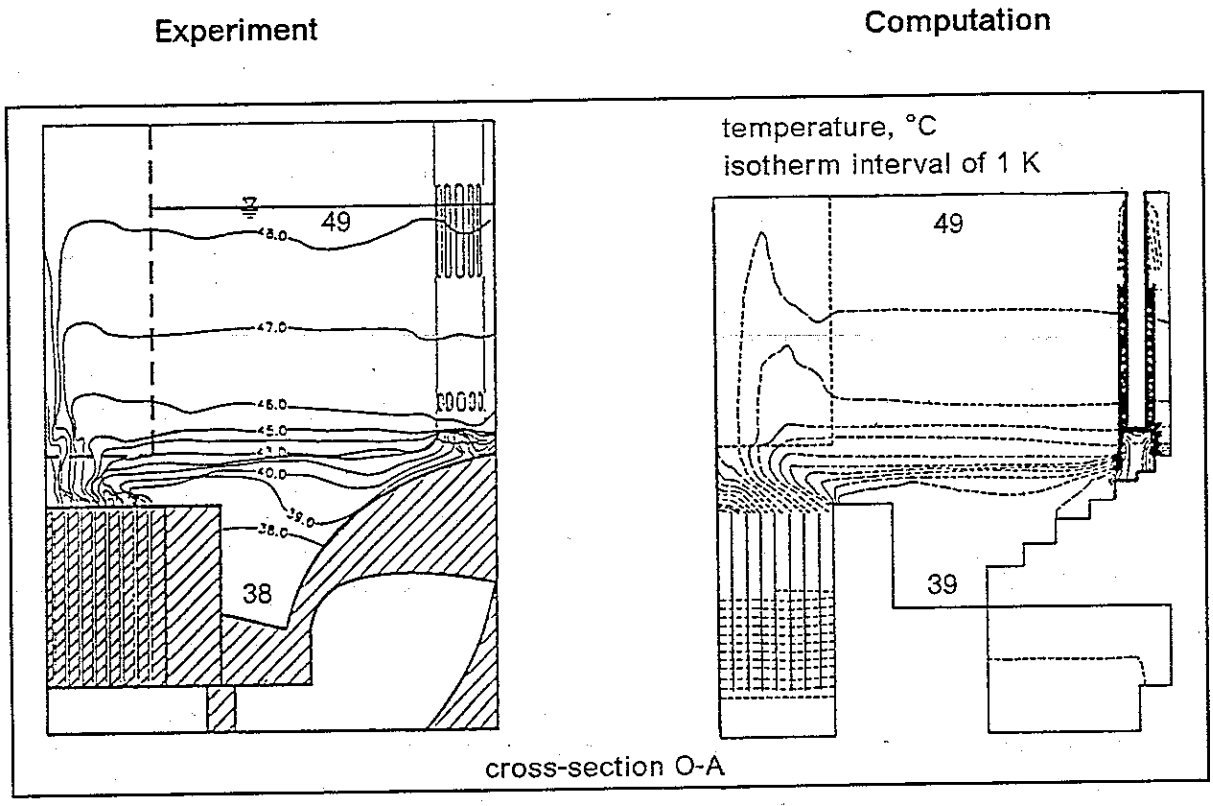

a) Test RA.S1: permeable ACS shell.

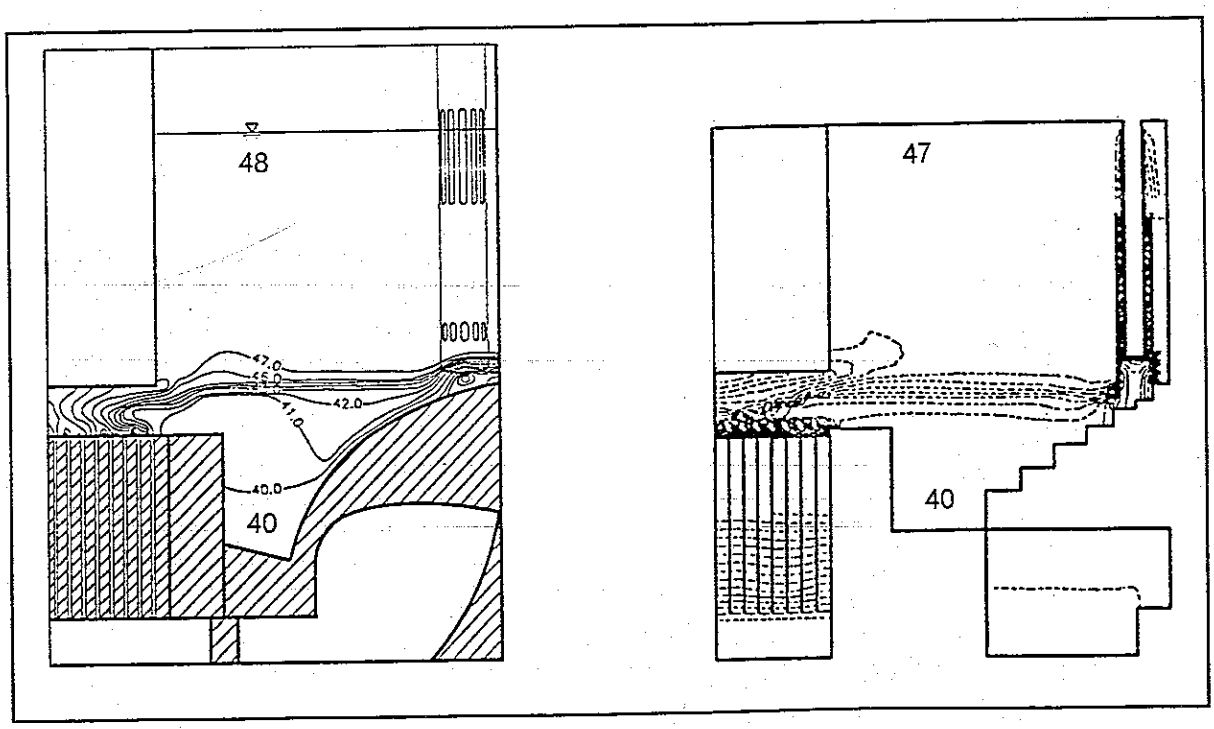

b) Test RA.S2: impermeable ACS shell.

Fig. 16. Influence of the ACS shell design on the measured and computed isotherm fields, tests RA.S1 and RA.S2.

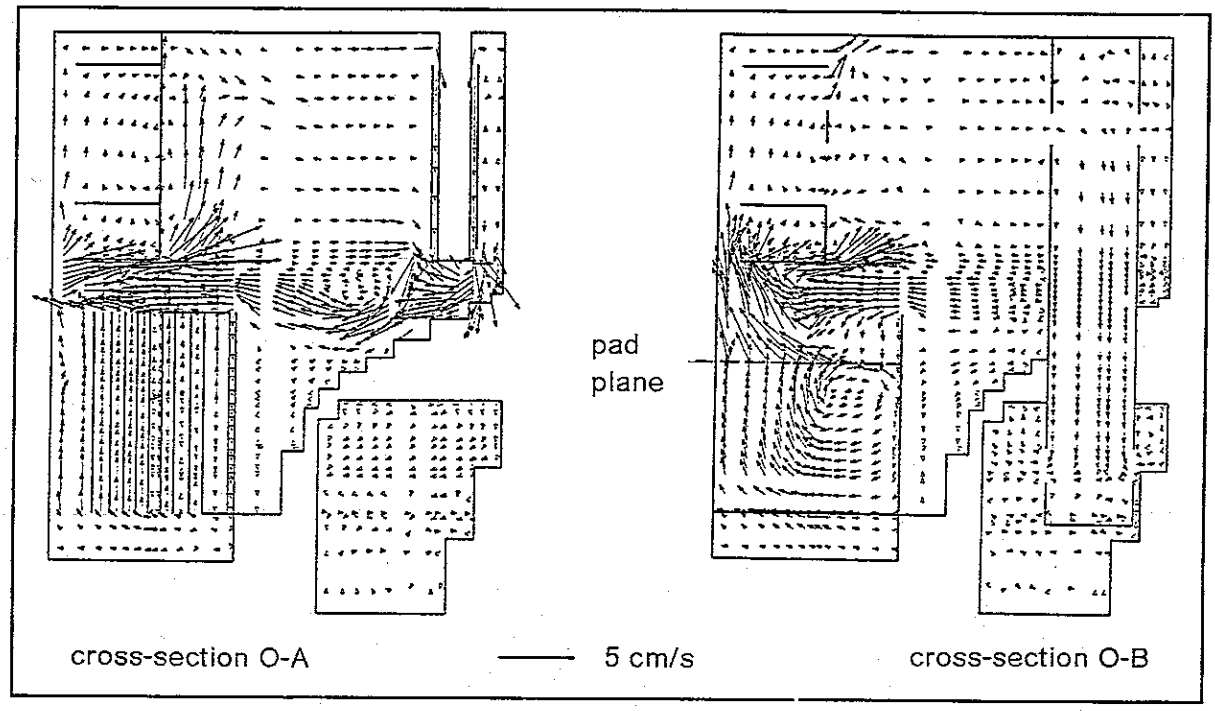

a) Test NE.S1: permeable ACS shell.

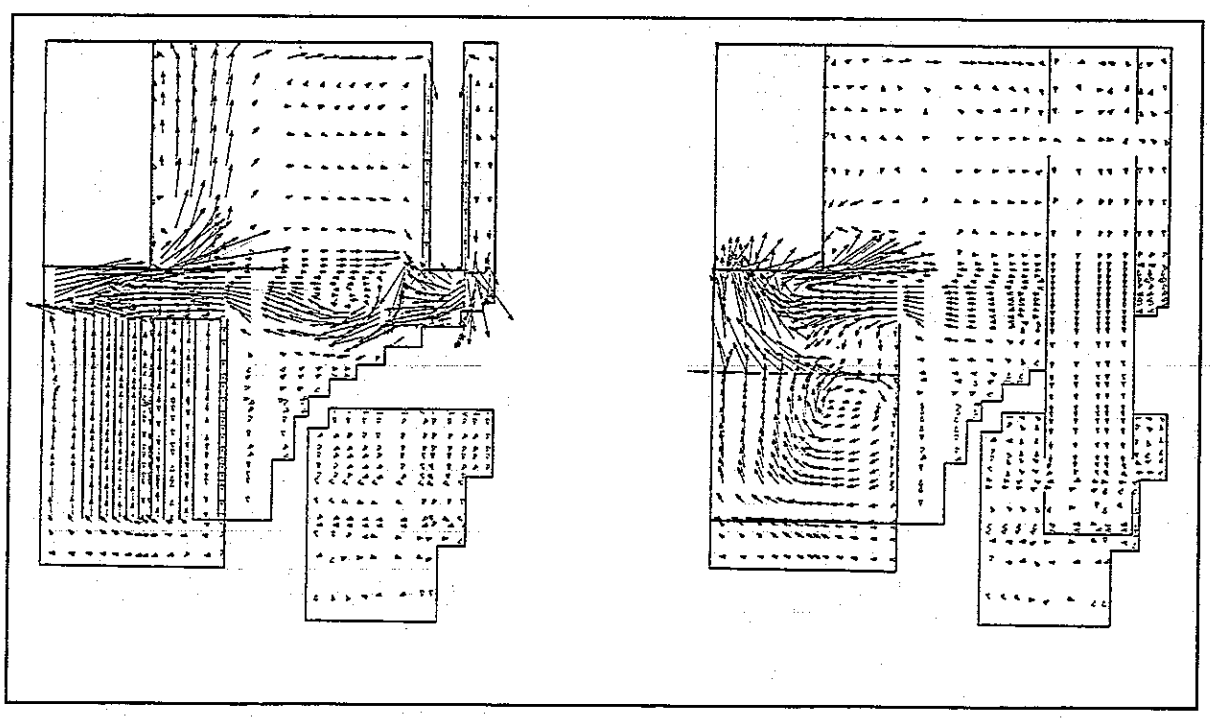

b) Test NE.S2: impermeable ACS shell.

Fig. 17. Influence of the ACS shell design on the computed velocity fields, tests NE.S1 and NE.S2.

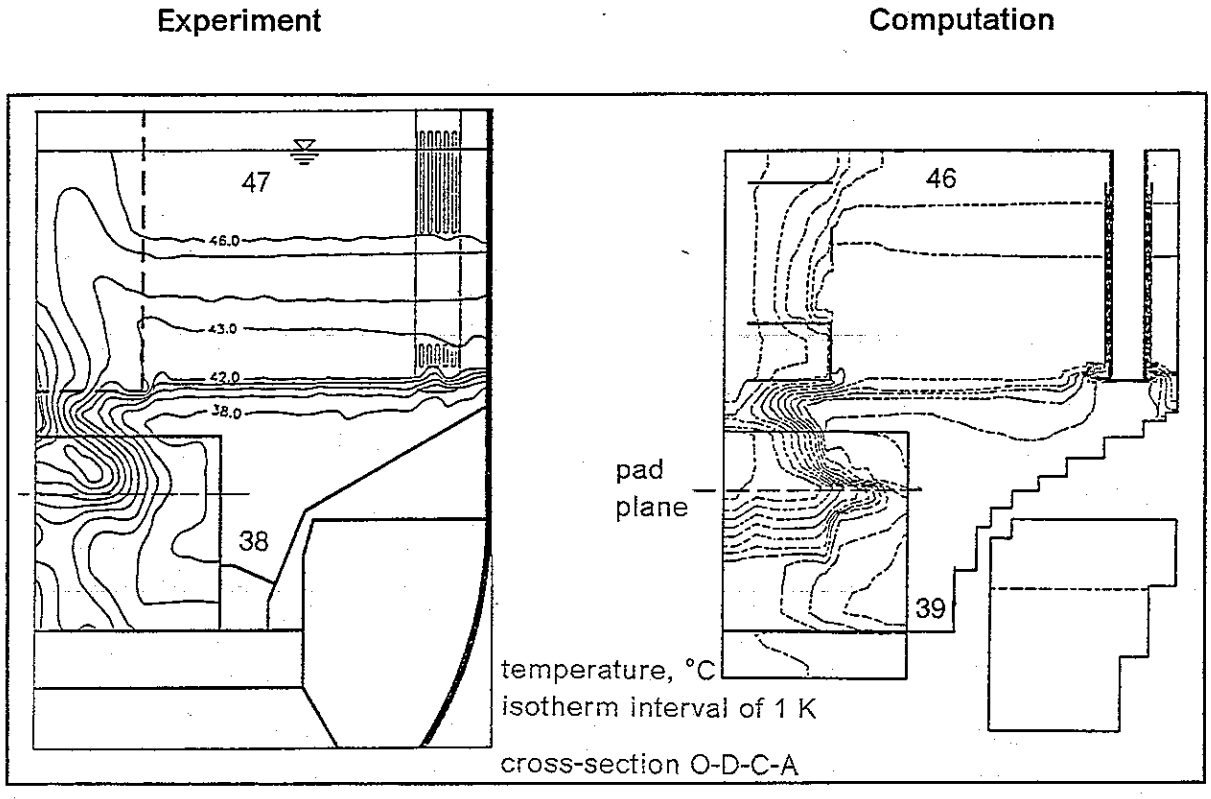

a) Test NE.S1: permeable ACS shell.

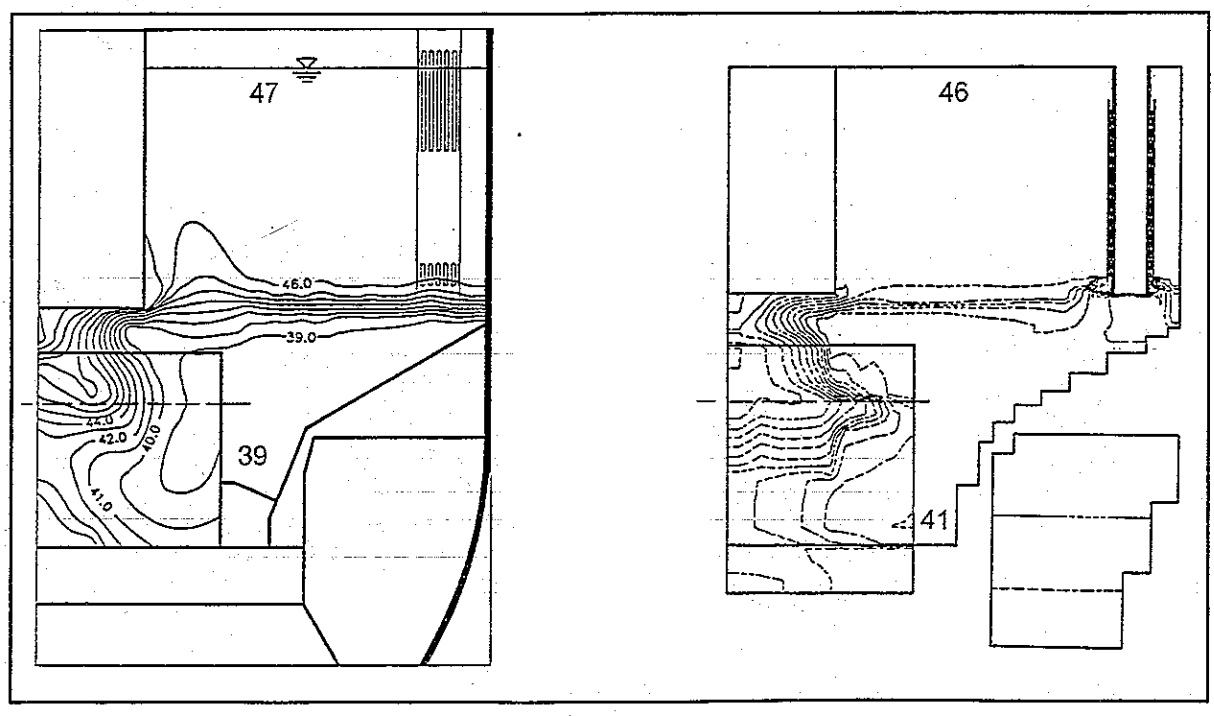

b) Test NE.S2: impermeable ACS shell.

Fig. 18. Influence of the ACS shell design on the measured and computed isotherm fields, tests NE.S1 and NE.S2.

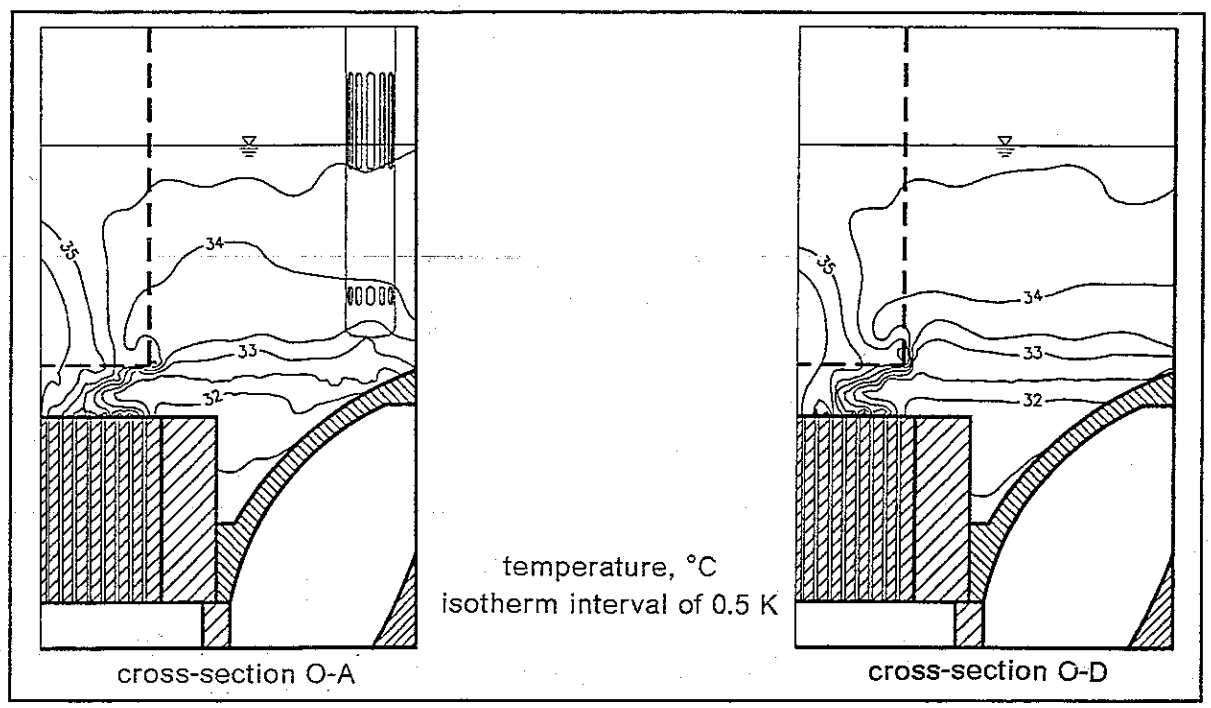

a) Test RA.S3: permeable ACS shell.

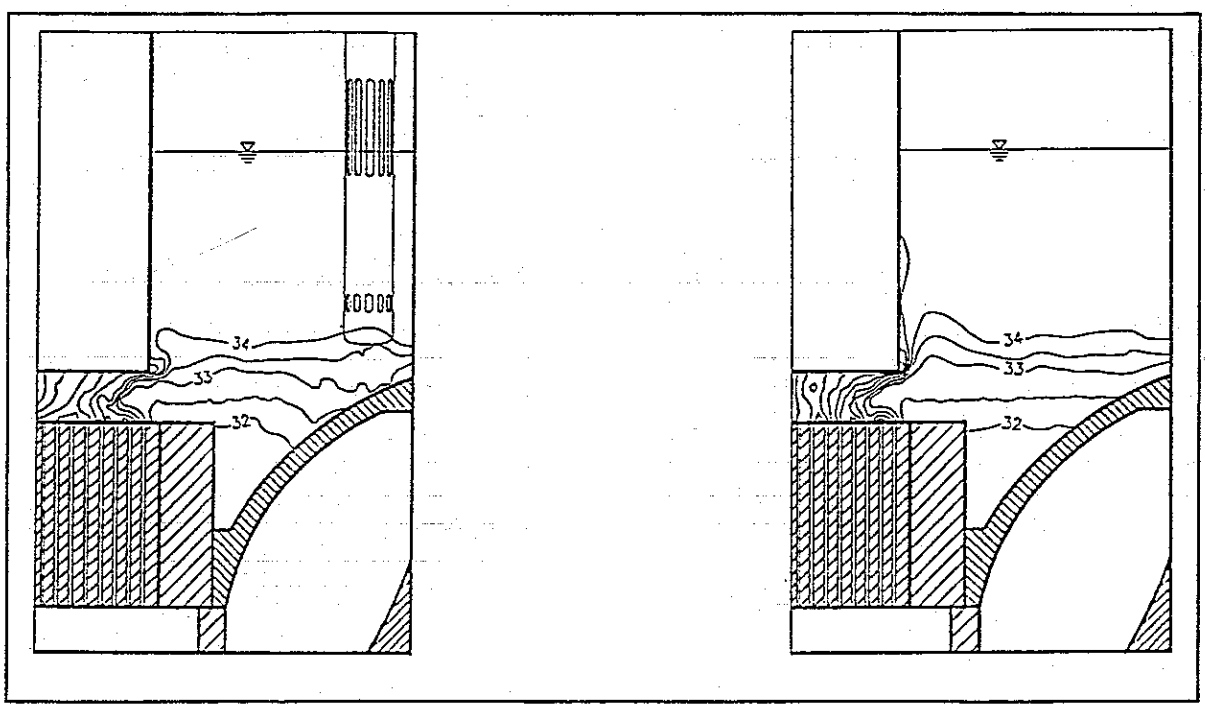

b) Test RA.S4: impermeable ACS shell.

Fig. 19. Influence of the ACS shell design on the isotherm fields measured in the RAMONA III setup, tests RA.S3 and RA.S4.

Test RA.T1 Test NE.T1

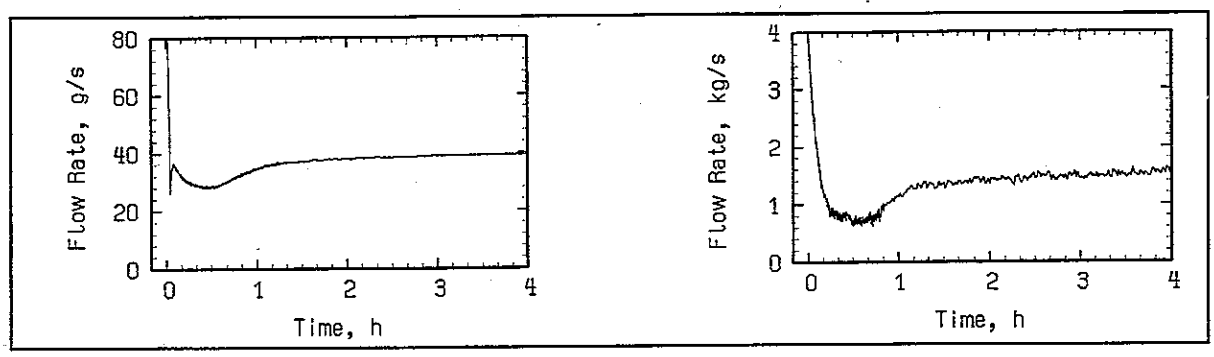

a) Total core mass flow rate.

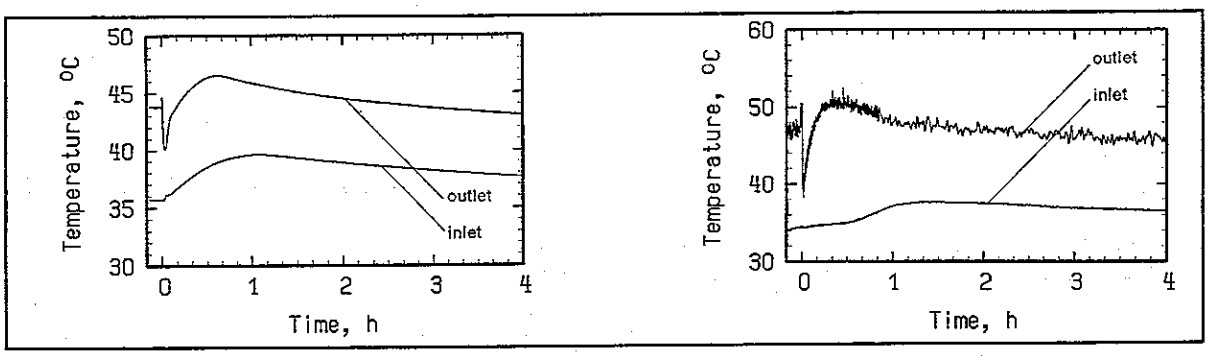

b) Temperatures at the core inlet and outlet side.

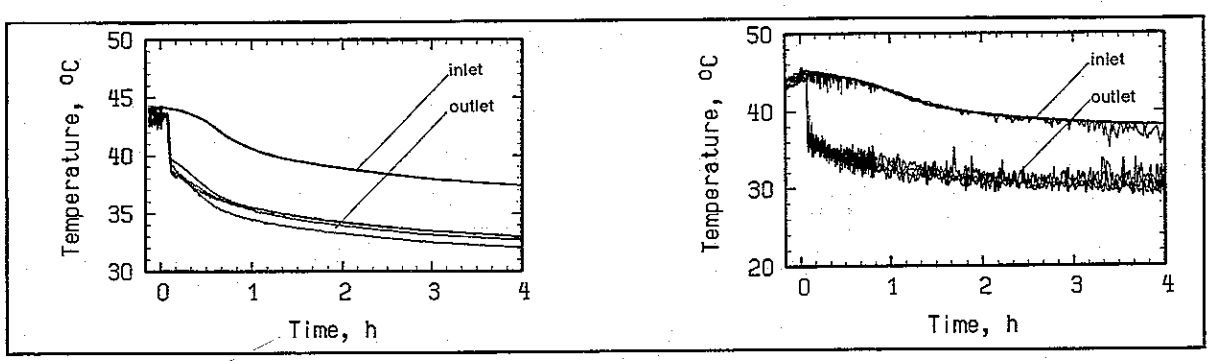

c) Temperatures at the DHX inlet and outlet side.

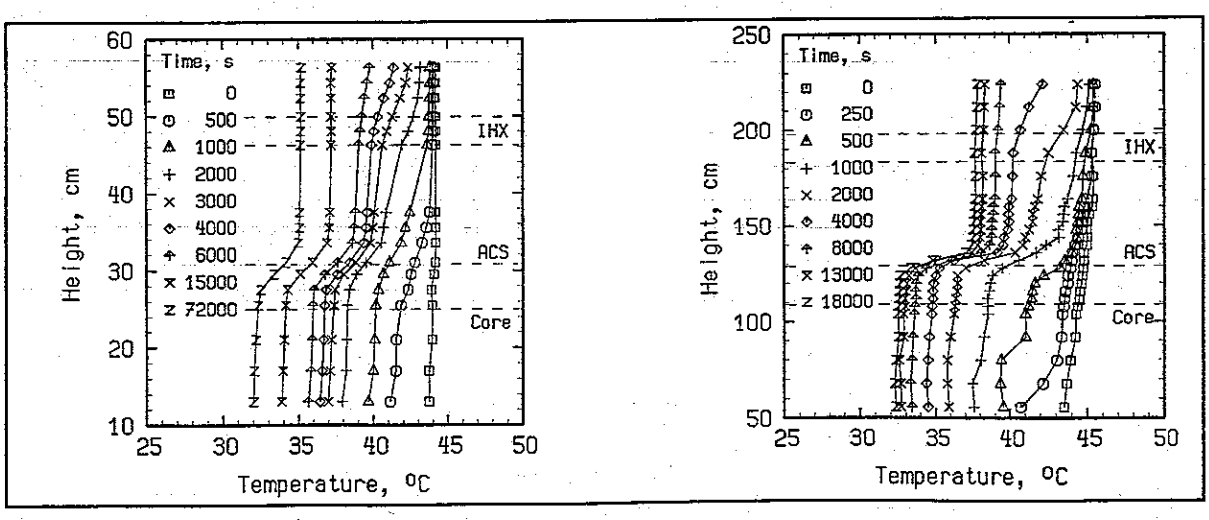

d) Temperature profiles in the upper plenum as function of the time after scram.

Fig. 20. Comparison of the baseline tests, tests RA.T1 and NE.T1.

Test RA.T2 Test NE.T2

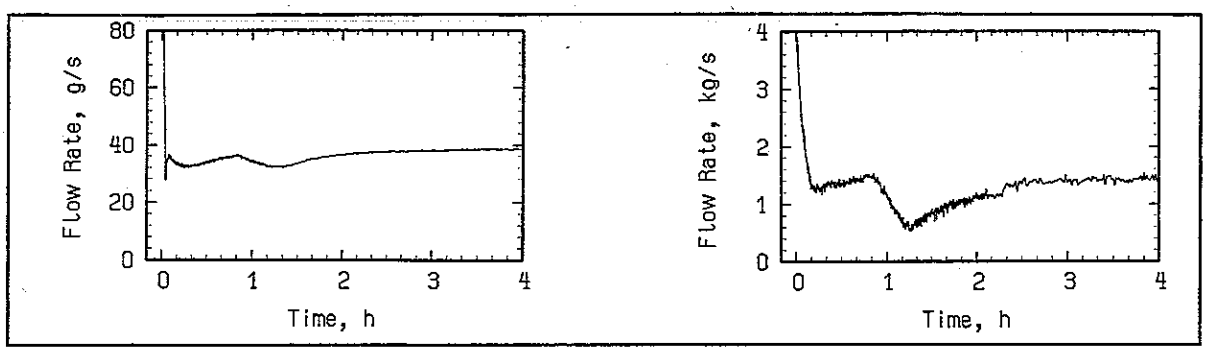

a) Total core mass flow rate.

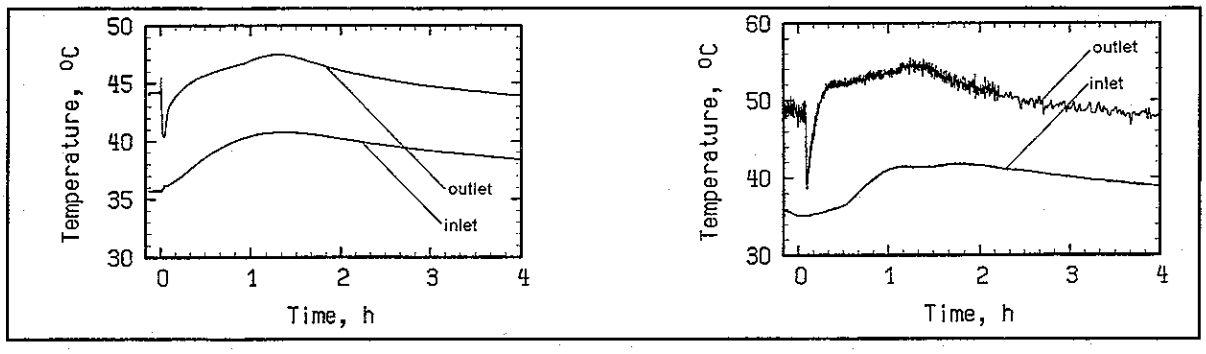

b) Temperatures at the core inlet and outlet side.

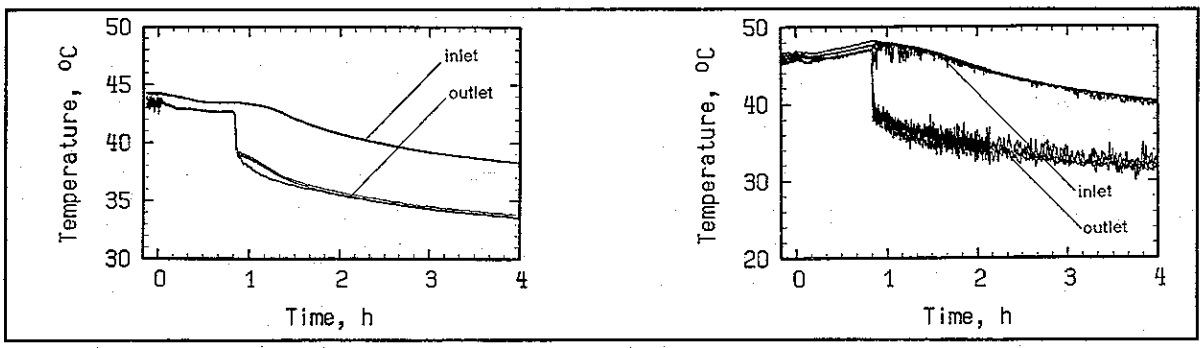

c) Temperatures at the DHX inlet and outlet side.

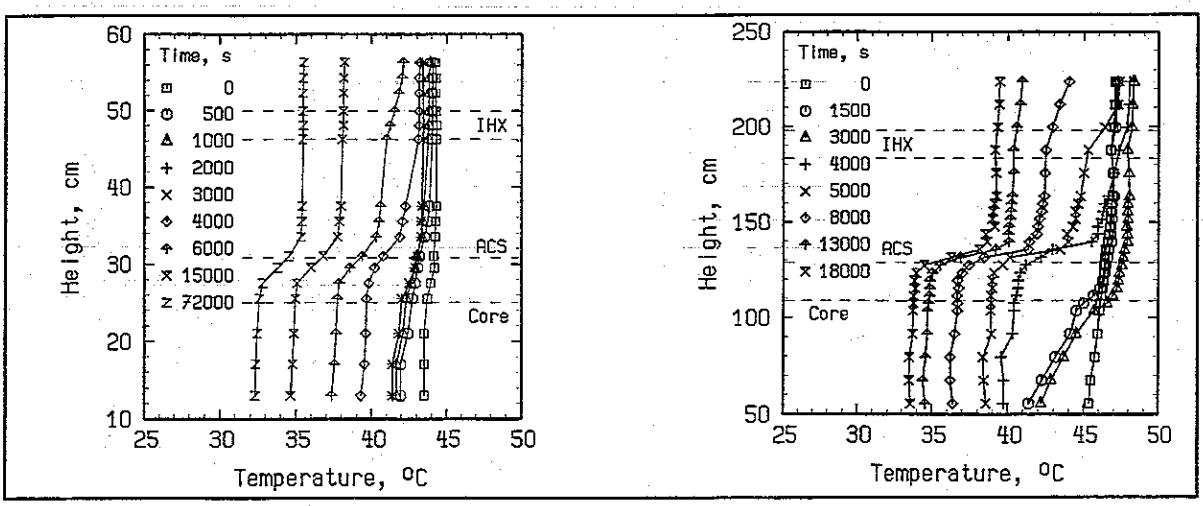

d) Temperature profiles in the upper plenum as function of the time after scram.

Fig. 21. Influence of a delayed DHX startup time, tests RA.T2 and NE.T2.

Test RA.T3 Test NE.T3

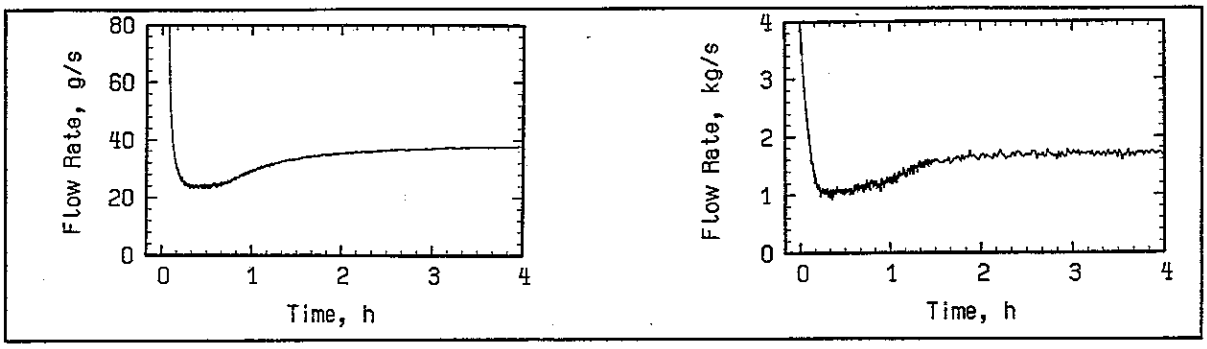

a) Total core mass flow rate.

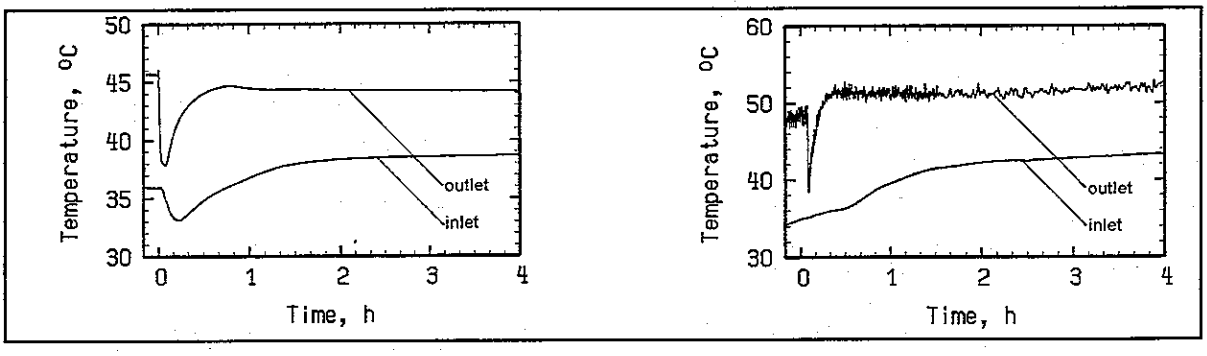

b) Temperatures at the core inlet and outlet side.

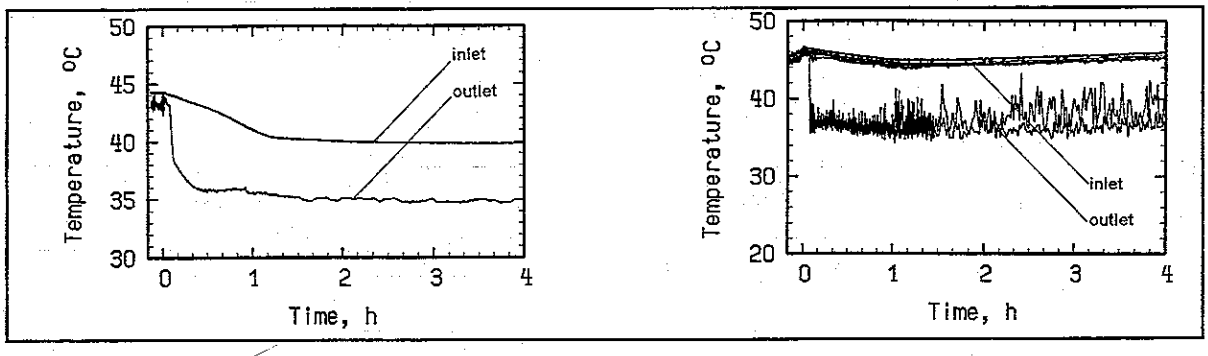

c) Temperatures at the DHX inlet and outlet side.

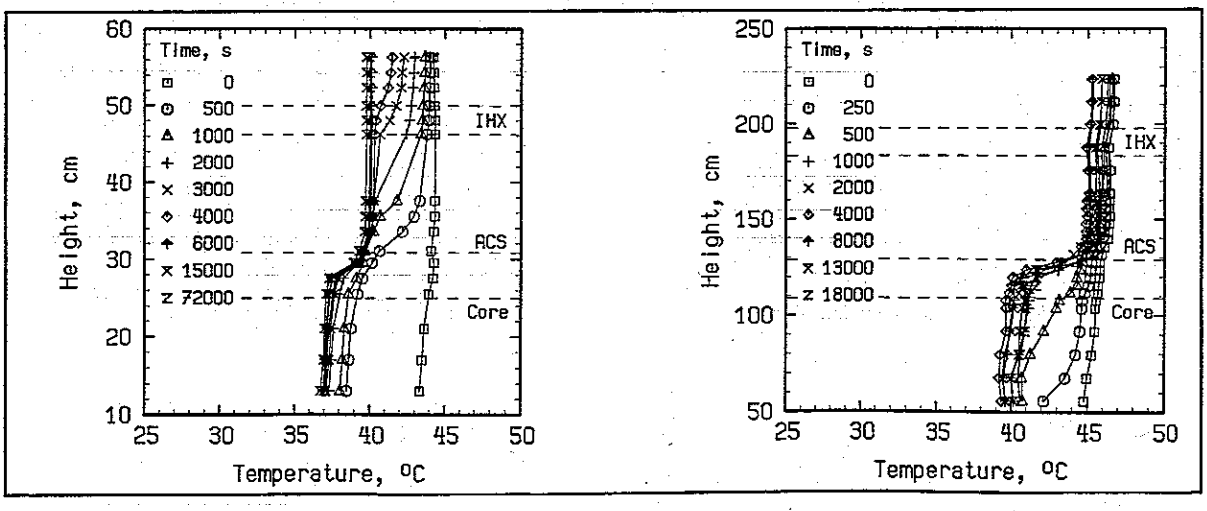

d) Temperature profiles in the upper plenum as function of the time after scram.

Fig. 22. Influence of a complete failure of two neighboring DHX circuits, tests RA.T3 and NE.T3.

Test RA.T5: RAMONA II

Test RA.T6: RAMONA III

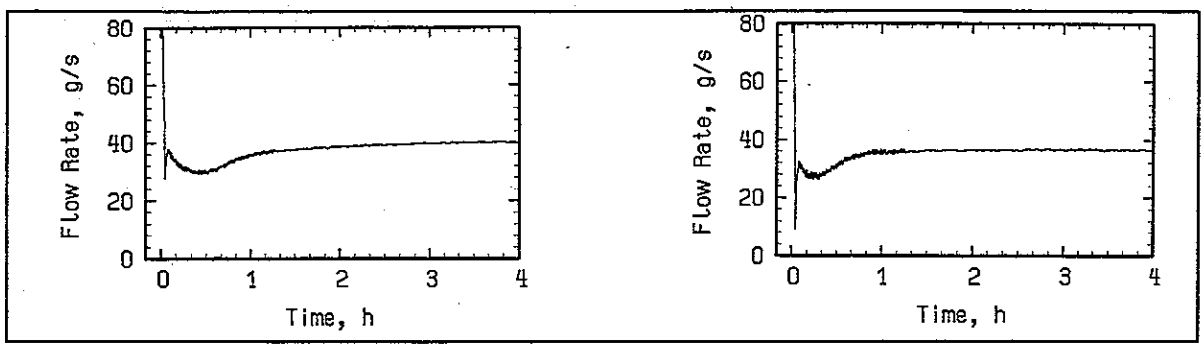

a) Total core mass flow rate.

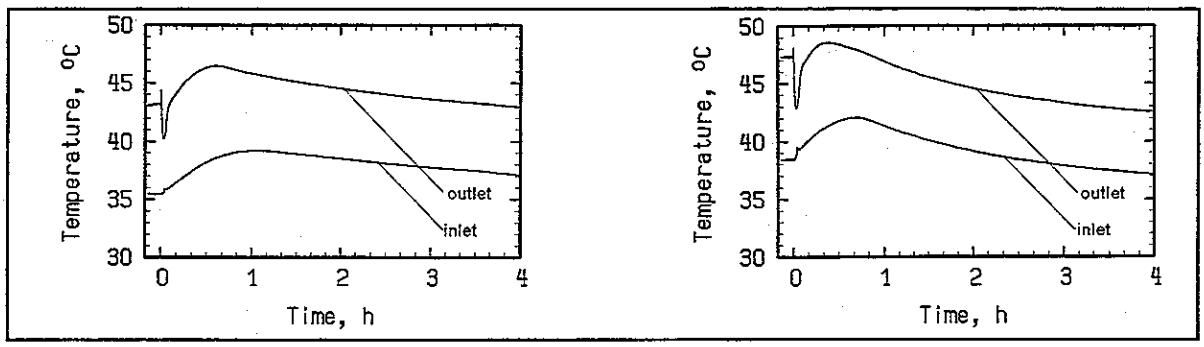

b) Temperatures at the core inlet and outlet side.

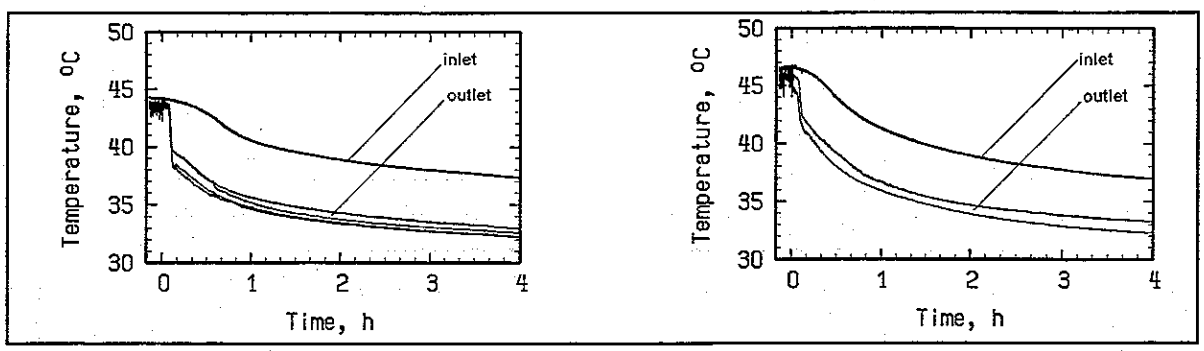

c) Temperatures at the DHX inlet and outlet side.

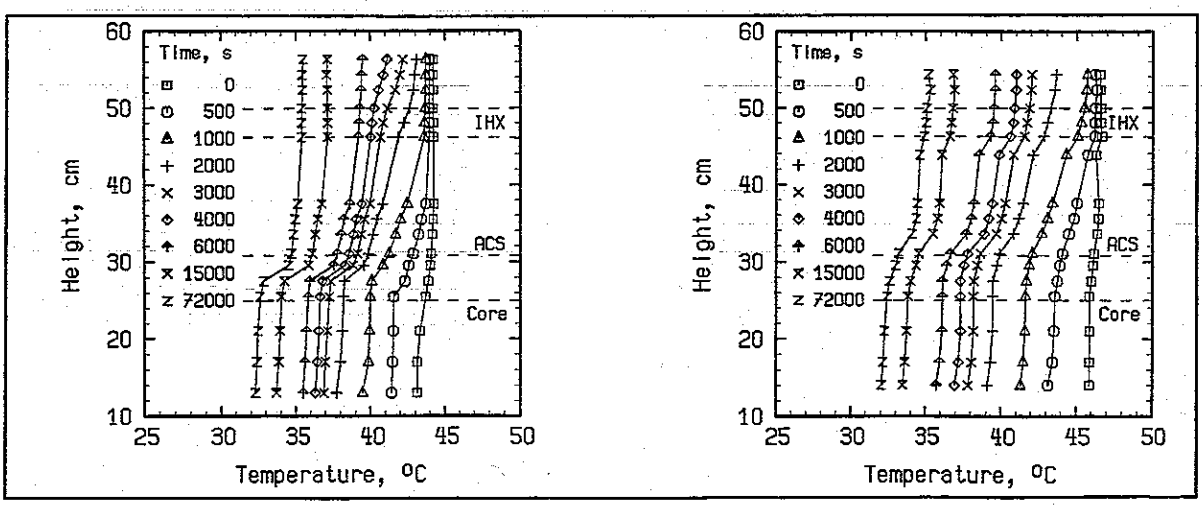

d) Temperature profiles in the upper plenum as function of the time after scram.

Fig. 23. Influence of the number of the installed heat transfer loops, tests RA.T5 (RAMONA II, four loops) and RA.T6 (RAMONA III, three loops).

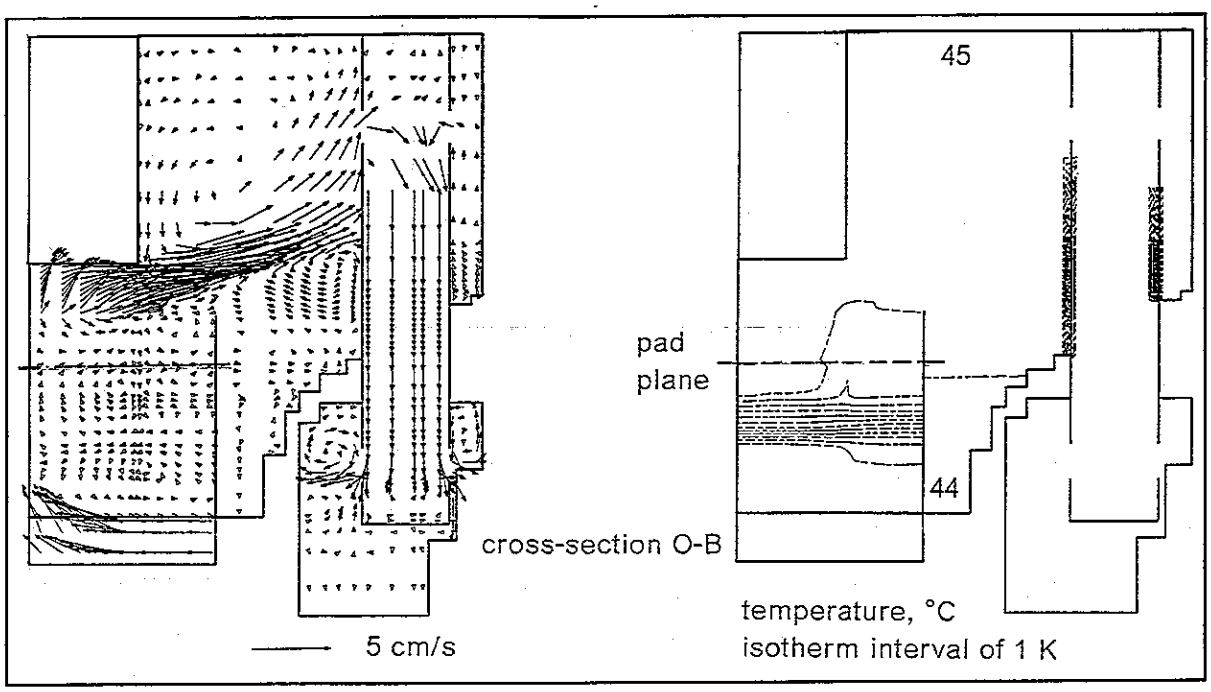

Fig. 24. Influence of a complete flow path blockage of the IHX primary sides on the computed velocity and isotherm fields (before initiation of scram), test NE.T4.

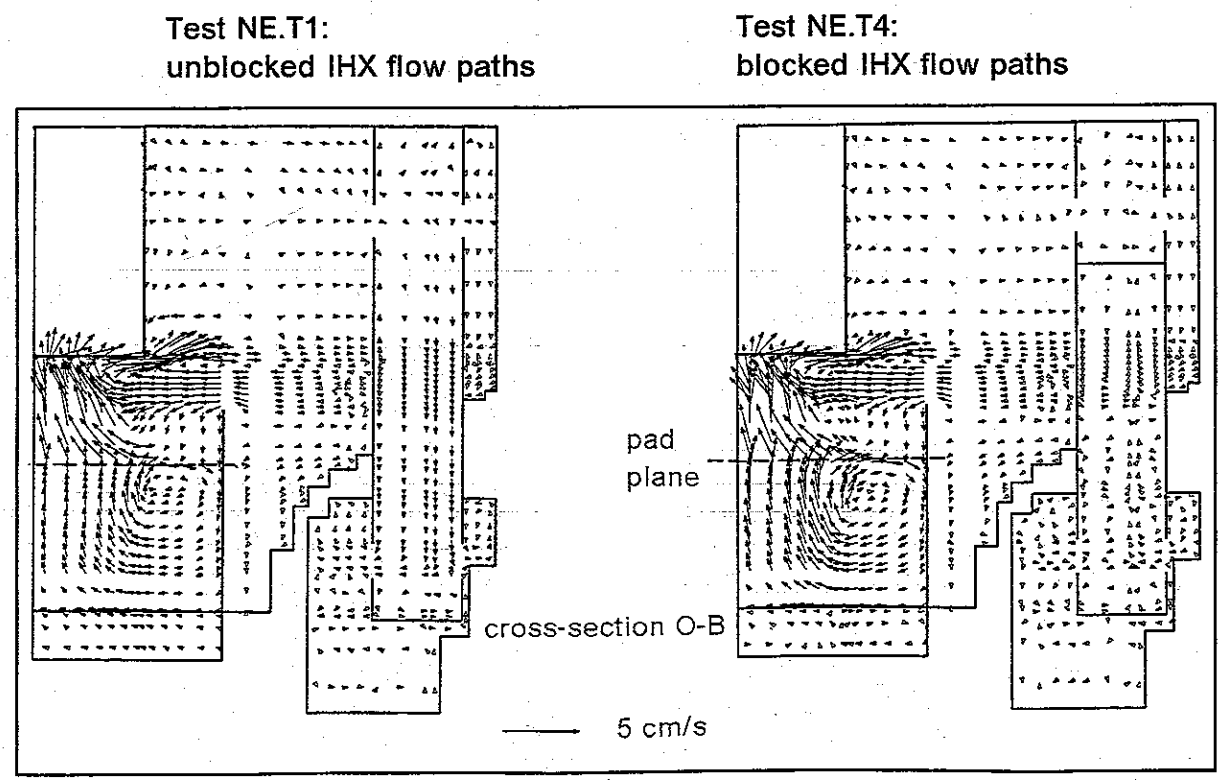

Fig. 25. Influence of a complete flow path blockage of the IHX primary sides on the computed velocity fields (at 18,000 s after initiation of scram), tests NE.T1 and NE.T4.

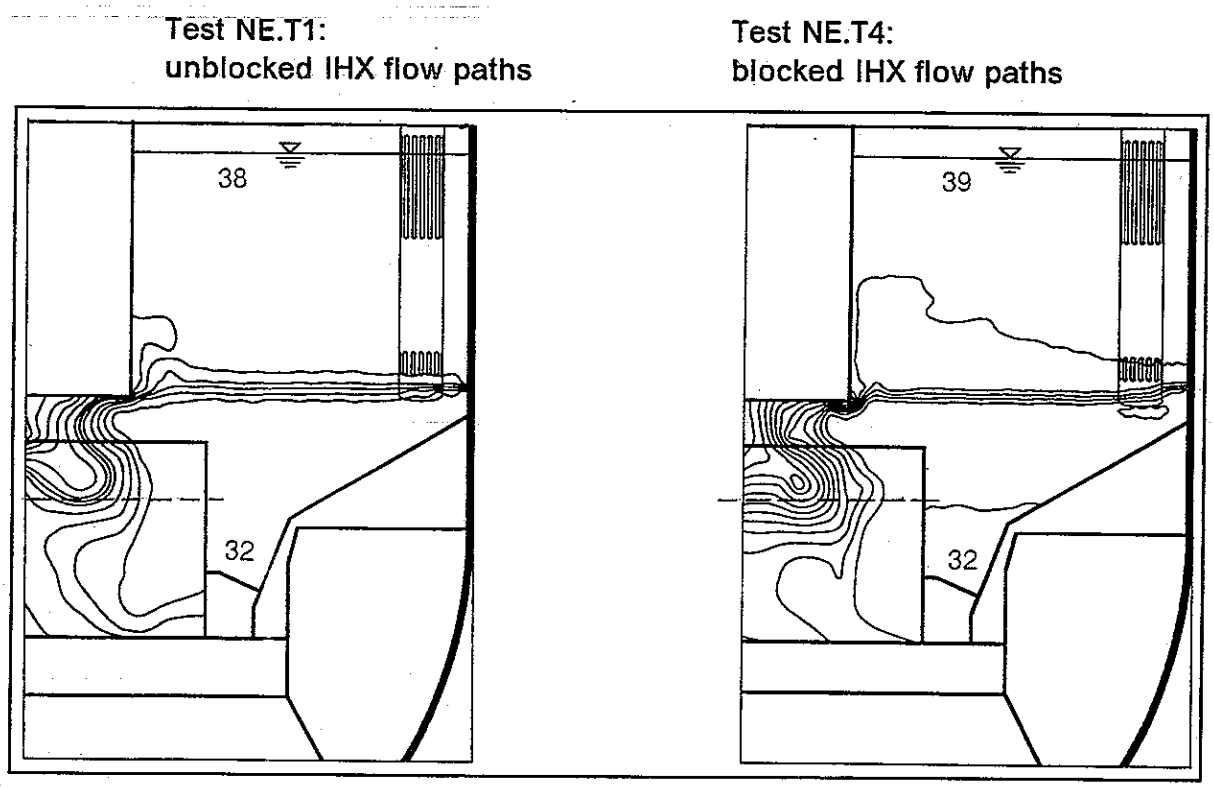

a) Experiment.

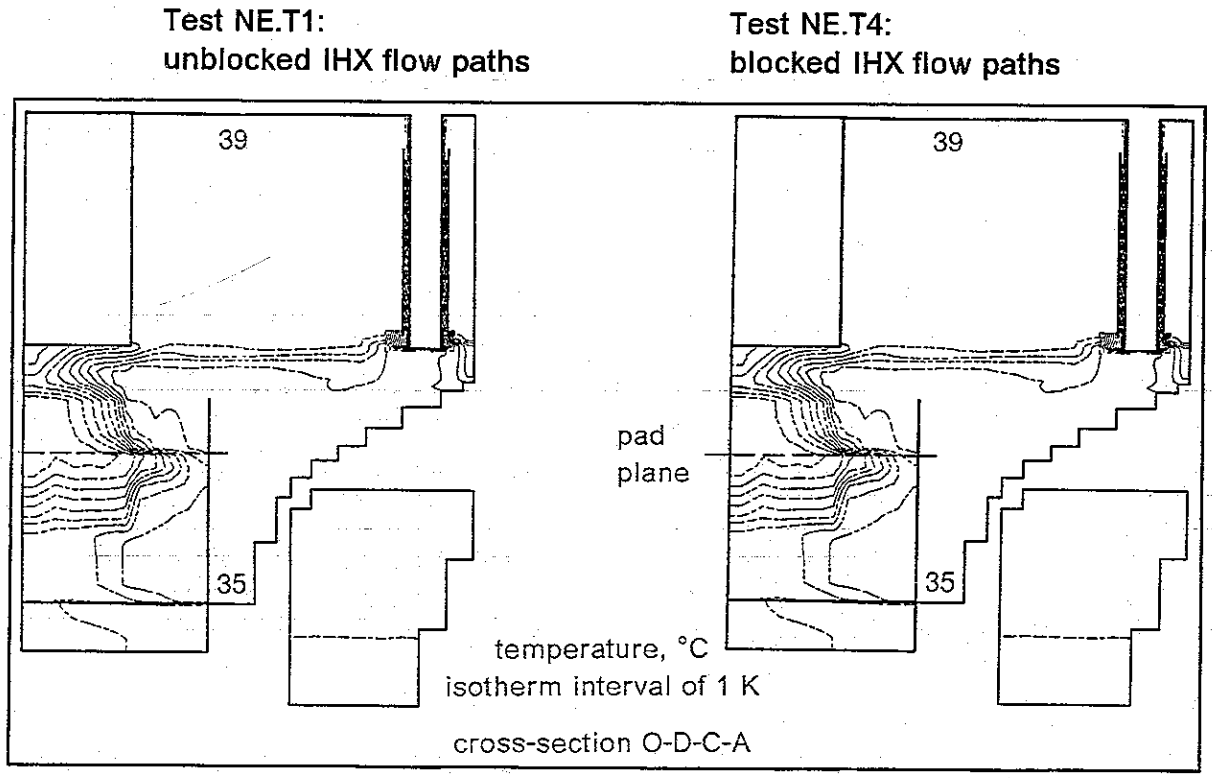

b) Computation.

Fig. 26. Influence of a complete flow path blockage of the IHX primary sides on the measured and computed isotherm fields (at 18,000 s after initiation of scram), test NE.T1 and NE.T4.

Test NE.T1
unblocked IHX flow paths

Test NE.T4
blocked IHX flow paths

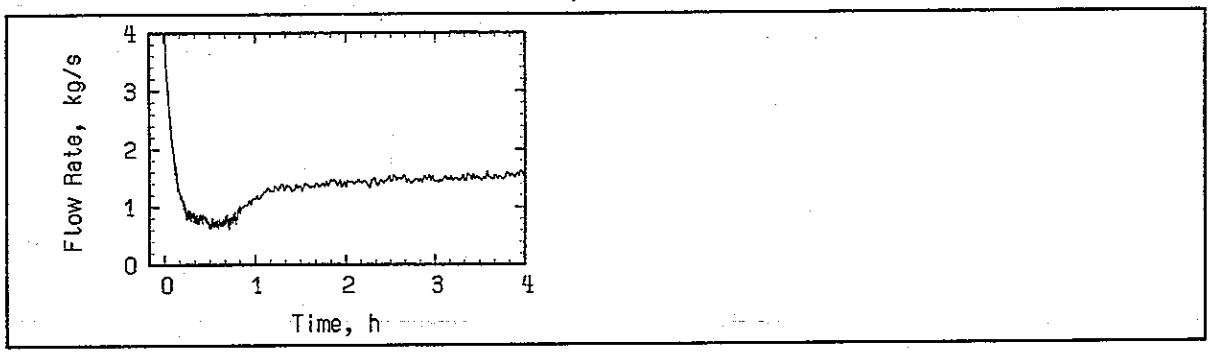

a) Total core mass flow rate.

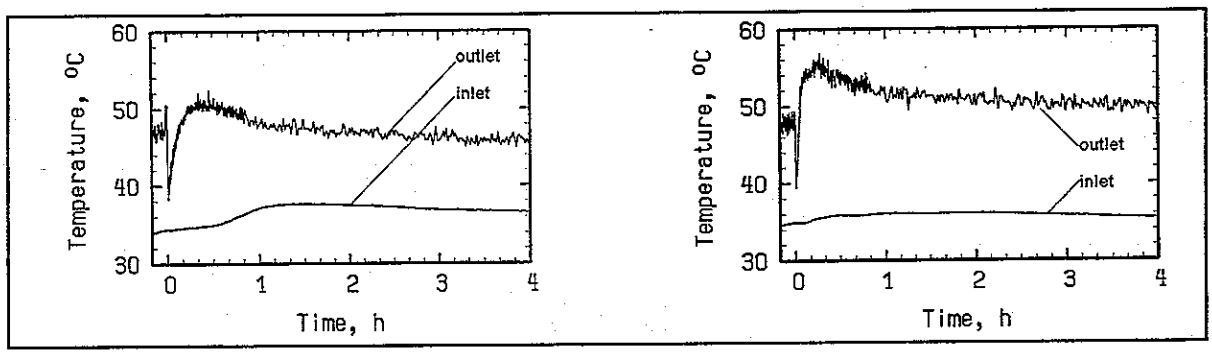

b) Temperatures at the core inlet and outlet side.

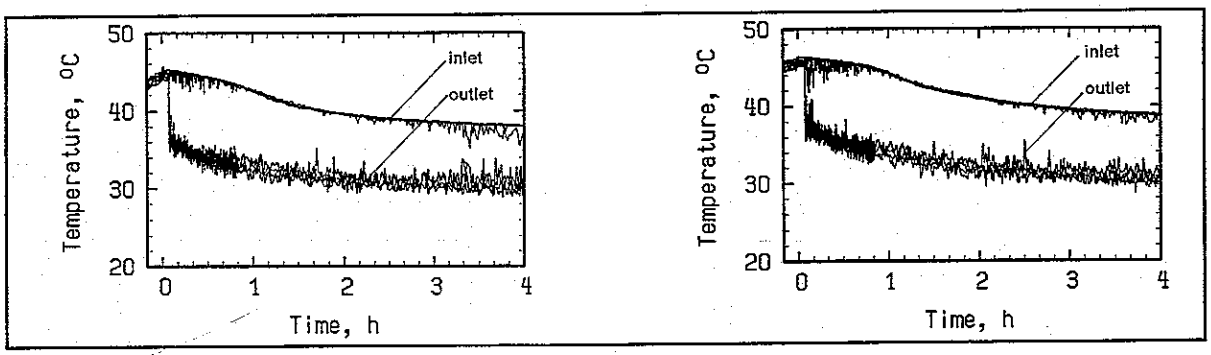

c) Temperatures at the DHX inlet and outlet side.

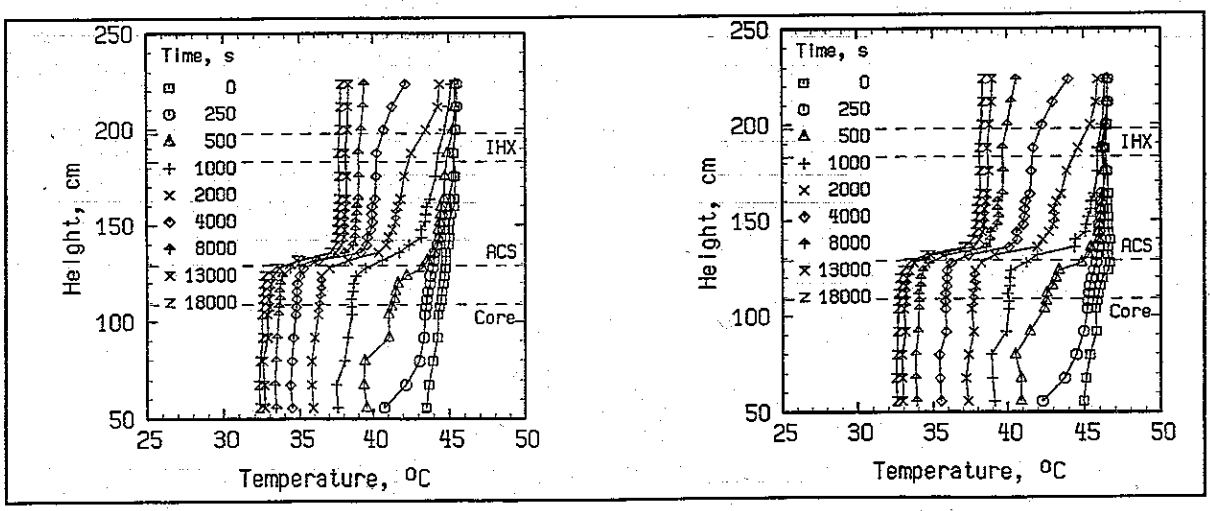

d) Temperature profiles in the upper plenum as function of the time after scram.

Fig. 27. Influence of a complete flow path blockage of the IHX primary sides, tests NE.T1 and NE.T4.

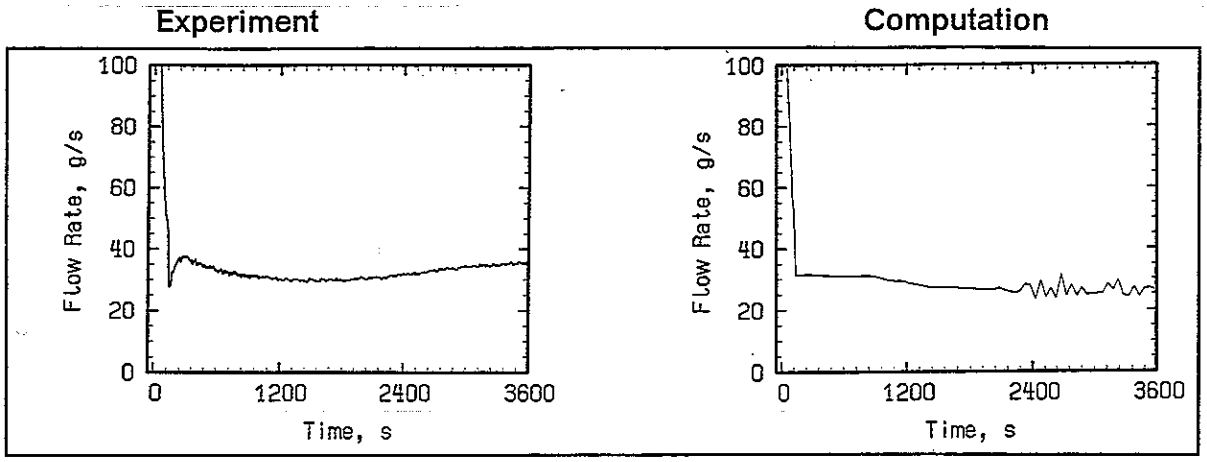

a) Total core mass flow rate.

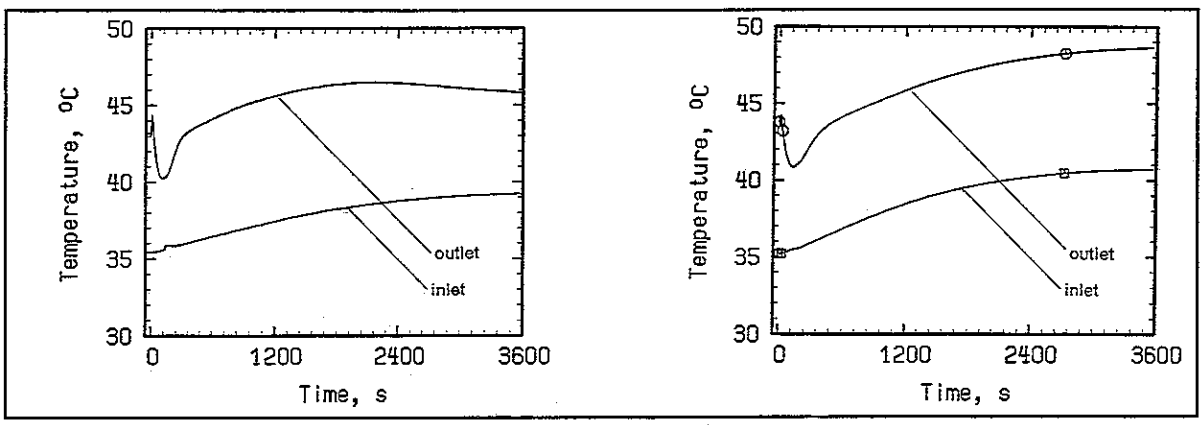

b) Temperatures at the core inlet and outlet side.

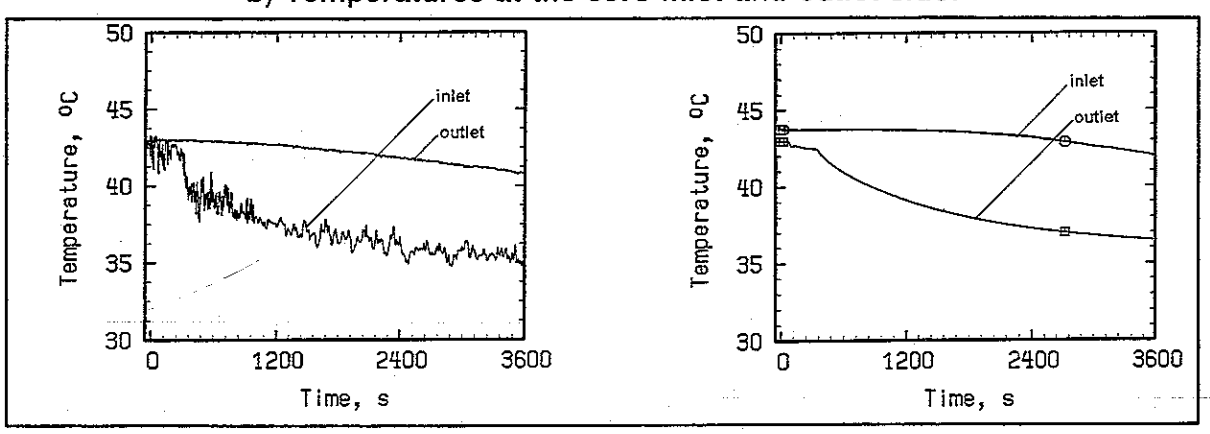

c) Temperatures at the DHX inlet and outlet side.

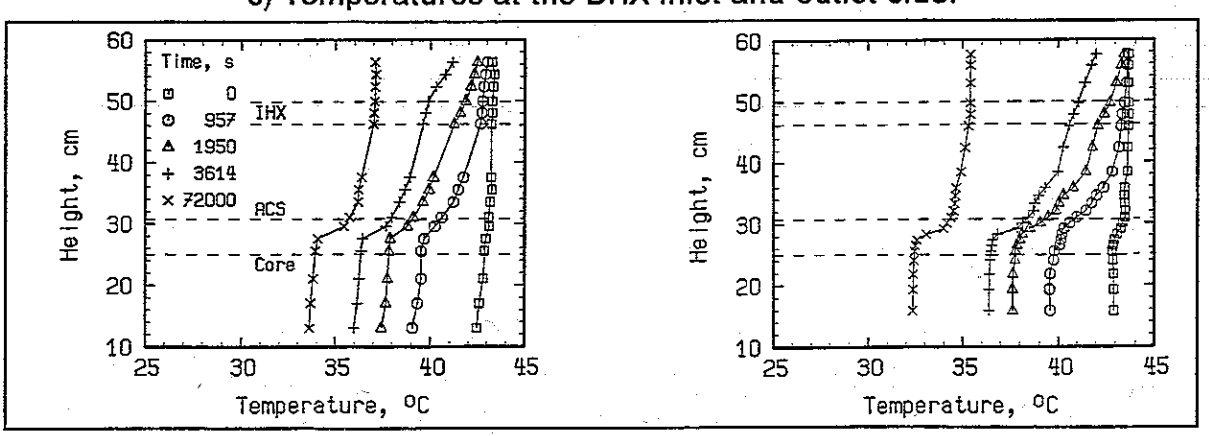

d) Temperature profiles in the upper plenum as function of the time after scram.

Fig. 28. Comparison of computed against experimental results, test RA.T4.